Geochimica Et Cosmochimica Acta
January 2020, Volume 269 Pages 346-375
https://doi.org/10.1016/j.gca.2019.09.038
https://archimer.ifremer.fr/doc/00599/71067/

Trace element proxies of seafloor hydrothermal fluids based on secondary ion mass spectrometry (SIMS) of black smoker chimney linings

Evans Guy N. [1, *], Tivey Margaret K. [1], Monteleone Brian [1], Shimizu Nobumichi [1], Seewald Jeffrey S. [1], Rouxel Olivier [2]

[1] Woods Hole Oceanog Inst, 360 Woods Hole Rd, Woods Hole, MA 02543 USA.
[2] Inst Francais Rech Exploitat Mer, Ctr Brest, Technopole Brest Iroise, Marine Geosci Unit, Plouzane, France.

* Corresponding author : Guy N. Evans, email address : gevans@framingham.edu; mktivey@whoi.edu

bmonteleone@whoi.edu ; nshimizu@whoi.edu ; jseewald@whoi.edu; orouxel@ifremer.fr

Abstract :

Sampling of paired black smoker chimney linings and seafloor hydrothermal vent fluids supports the development of trace element proxies for sulfide mineral deposition environments by facilitating analyses of trace element partitioning between mineral and fluid phases under well-constrained physiochemical conditions. Here, concentrations of Co, Ni, Ga, Ag, and In in chalcopyrite lining 22 black smoker chimneys (29 for Co, Ag, and In) are measured using secondary ion mass spectrometry (SIMS) calibrated against inductively coupled plasma mass spectrometry (ICP-MS) and NIST-traceable reference solutions. To provide additional data on the trace element concentrations of vent fluid pairs for 19 of the 29 black smoker chimney linings investigated, this paper also presents new ICP-MS data for 33 hydrothermal vent fluids collected from the Tahi Moana-1, ABE, Tu'i Malila, and Mariner vent fields on the Eastern Lau Spreading Center and Valu Fa Ridge.

The chalcopyrite black smoker chimney linings investigated represent a variety of temperature (269-395 degrees C), chemical (e.g., pH (at 25 degrees C) = 2.3-4.4), and geologic conditions. Electron microprobe results indicate that mineral stoichiometry ranges from stoichiometric chalcopyrite to mol Cu : mol Fe = 0.65. Trace element concentrations obtained by SIMS are: Co (<2 ng/g-760 mu g/g), Ni (<17 ng/g-454 mu g/g), Ga (<0.9 ng/g-48 mu g/g), Ag (60 mu g/g-3800 mu g/g), In (<0.5 ng/g-270 mu g/g). Concentrations of Ag in chalcopyrite strongly correlate with the free ion activity ratio of {Ag+}:{Cu+} in paired vent fluids, with high Ag concentrations in chalcopyrite indicating formation from near neutral vent fluids containing low Cu concentrations or low-pH vent fluids with high Ag concentrations attributable to subsurface Ag remobilization. Chalcopyrite with low Ag precipitates from low-pH Cu-rich fluids unaffected by extensive Ag remobilization. Concentrations of Ga and In in chalcopyrite exhibit a negative trend with vent fluid pH, possibly reflecting the strength of Ga and In OH- complexes. Thus, Ga and In concentrations differentiate Ag-rich chalcopyrite formed from near-neutral Cu-poor vent fluids or that formed from Ag-rich

low-pH vent fluids. In contrast, Co and Ni exhibit no trend with fluid data, but correlate with mineral Cu:Fe ratios, possibly reflecting the greater availability of Fe(II) lattice sites or paired substitution of 2+ ions.

Overall, this study demonstrates the potential of paired vent fluid and black smoker chimney samples to provide insight into the partitioning of trace elements in sulfide mineral deposition environments and related proxies of important fluid parameters such as pH and metal concentrations. This study also demonstrates the utility of SIMS to precisely analyze trace elements in chalcopyrite at high spatial resolutions and low detection limits.

Keywords : Seafloor massive sulfide, Chalcopyrite, Ore, Mineral, pH

1. INTRODUCTION

Deep-sea hydrothermal vents are unique locations where actively forming seafloor massive sulfide (SMS) deposits and venting hydrothermal fluids can be directly accessed and sampled. However, SMS deposits and hydrothermal vent fluids are often sampled, analyzed, and reported in separate studies causing information about the correspondence between SMS deposit chemistry and corresponding hydrothermal vent fluids to be lost or overlooked. Systematic collection and analyses of paired SMS deposit and hydrothermal fluid samples provide detailed constraints on the formation conditions of SMS deposits. For example, previous studies have quantitatively investigated the fractionation of stable sulfur and metal isotopes and the partitioning of trace elements between hydrothermal fluids and sulfide minerals (e.g., Ono et al., 2007; Rouxel et al., 2008; John et al., 2008; McDermott et al., 2015).

To further investigate trace element partitioning between hydrothermal vent fluids and sulfide mineral deposits, this study focuses on precise trace element analyses of the innermost linings of black smoker chimneys. Because these linings formed in direct contact with venting hydrothermal fluids, their chemistry can be expected to reflect the physiochemical conditions imposed by the fluids. Previous analyses of several of the black smoker chimney linings investigated here have shown that these linings are in close sulfur-isotopic equilibrium with corresponding hydrothermal vent fluids (McDermott et al., 2015).

Models for the formation of black smoker chimney deposits typically differentiate between two major stages of deposit formation (Haymon, 1983; Goldfarb et al., 1983). First, heating of seawater by venting hydrothermal fluids leads to the precipitation of an initial chimney wall dominantly composed of anhydrite ($CaSO_4$), with metal sulfide minerals occurring as interstitial grains. Following physical and chemical separation of venting hydrothermal fluids

from surrounding seawater by the initial chimney wall, a second stage of black smoker chimney formation is characterized by precipitation of a massive sulfide lining along the interior surface of the chimney wall and concentric zonation within the wall as minerals continue to dissolve and precipitate according to steep temperature and chemical gradients (Fig. 1A). Above ~250°C, second-stage massive sulfide linings typically contain chalcopyrite ($CuFeS_2$) or a Cu-Fe-S intermediate solid solution with a chemical composition between that of chalcopyrite and isocubanite ($CuFe_2S_3$) (Haymon, 1983; Goldfarb et al., 1983). Zinc-iron sulfides ((Zn,Fe)S) such as wurtzite and sphalerite are also common, especially at lower temperatures. Iron-sulfides, pyrite/marcasite (FeS_2) and pyrrhotite ($Fe_{(1-x)}S_x$), are likewise common within chimney walls, but are rarely found along the interior surfaces of black smoker chimneys in direct contact with hydrothermal vent fluids.

Previous studies have noted a close correspondence between the mineralogy of second-stage black smoker chimney linings and vent fluid characteristics including temperature, sulfur fugacity, and pH (e.g., Tivey, 1995; Tivey et al., 1999; Kawasumi and Chiba, 2017; Evans et al., 2017). However, these mineralogical indicators can only distinguish between broad ranges of temperature and chemical composition. Analyses of trace elements in black smoker chimney linings provide an additional and potentially more precise indicator of vent fluid temperatures and chemistry. For example, the Fe content of sphalerite and wurtzite has been demonstrated to closely reflect vent fluid temperature and sulfur fugacity, which is subsequently indicative of vent fluid H_2 concentrations (e.g., Hannington et al., 1995; Keith et al., 2014; Kawasumi and Chiba, 2017). Similarly, the trace element contents of pyrite in SMS deposits have been related to the physiochemical parameters of hydrothermal fluids, which are in turn related to geologic processes including fluid-sediment reactions, phase separation, subsurface mixing with seawater,

97 and magmatic volatile inputs (Keith et al., 2016). Such successes motivate the search for
98 additional trace element proxies concerning fundamental vent fluid characteristics such as
99 temperature, pH, and elemental concentrations.

100 The concentrations of many trace elements in chalcopyrite (and Cu-Fe-S intermediate
101 solid solutions) along the innermost linings of black smoker chimneys are at or below the ~100s
102 molar parts per million detection limits of electron microprobe (e.g., Tivey et al., 1995; Tivey et
103 al., 1999; Craddock, 2009; Evans et al., 2017). Techniques that offer lower detection limits, such
104 as laser ablation-inductively coupled plasma-mass spectrometry (LA-ICP-MS), proton
105 microprobe (PIXE), and secondary ion mass spectrometry (SIMS), have also been used to
106 investigate the composition of black smoker chimney linings (e.g., Butler and Nesbitt, 1999;
107 Ryan, 2001; Layne et al., 2005). However, these studies have been hampered by a lack of
108 suitable matrix-matched reference materials requiring results must to be reported in relative
109 rather than absolute concentrations (e.g., Butler and Nesbitt, 1999; Layne et al., 2005). More
110 recently, some LA-ICP-MS measurements of trace elements in sulfide minerals have been
111 calibrated using pressed sulfide powder precipitates, doped Li-borate glasses, or synthetic
112 sintered doped sulfides (Maslennikov et al., 2009, Danyshevsky et al., 2011; Wohlgemuth-
113 Ueberwasser et al., 2015). While these methods offer more reliable results reported as absolute
114 concentrations, understandings of the relationship between concentrations of trace elements in
115 hydrothermally precipitated sulfide minerals and corresponding hydrothermal fluids remain
116 imprecise.

117 This study investigates relationships between the trace element contents of copper-iron
118 sulfide minerals (primarily chalcopyrite) in black smoker chimney linings and paired
119 hydrothermal vent fluids from a selection of seafloor hydrothermal vent fields exhibiting a

variety of temperature and chemical characteristics. Trace element concentrations in black smoker chimney linings were measured using SIMS, which offers sufficiently high spatial resolution (spot diameter = 40 μm) and low detection limits (~ 1 ng/g) to analyze generally fine-grained and trace-element poor samples (Fig. 1B). To calibrate SIMS measurements against matrix-matched references materials, chalcopyrite grains were carefully picked from a subset of the black smoker chimney linings and analyzed by solution inductively coupled plasma mass spectrometry (ICP-MS) calibrated against NIST-traceable reference solutions. To normalize SIMS secondary ion ratios against major element concentrations and to investigate possible effects of mineral stoichiometry on trace element concentrations, selected samples were additionally analyzed by electron microprobe. The resulting data and comparisons between the trace element contents of black smoker chimney linings and the physiochemical parameters of paired hydrothermal vent fluids makes it possible to search for and identify trace element proxies of vent fluid parameters recorded in the chemistry of black smoker chimney linings.

2. SAMPLE DESCRIPTION

2.1. Black Smoker Chimney Linings

Black smoker chimney linings were obtained from samples stored at the Woods Hole Oceanographic Institution (WHOI). These samples were originally collected from active seafloor vent fields including those along the southern East Pacific Rise between 17°34'S and 17°37'S (AT-03, Leg 28), the Main Endeavour Field on the Juan de Fuca Ridge (AII-118, Leg 22; AT-03, Leg 30), the Lucky Strike vent field on the Mid-Atlantic Ridge (DIVA1), the Beebe/Piccard vent field on the Mid-Cayman Rise (AT18-16), the Vienna Woods, Fenway, Satanic Mills, Roman Ruins, Roger's Ruins, Suzette, and North Su vent fields in the Manus Basin (MGLN06MV), and

the Tahi Moana-1, ABE, Tu'i Malila, and Mariner vent fields in the Lau Basin (TN236; RR1507). Together, these samples represent a variety of geologic settings including fast-spreading (southern East Pacific Rise), intermediate-spreading (Endeavour Segment of the Juan de Fuca Ridge), slow-spreading (Lucky Strike), and ultraslow-spreading (Mid-Cayman Rise) mid-ocean ridges, and back-arc basins (Lau Basin and Manus Basin), covering a range of vent fluid temperatures (274–395°C), pH ($pH_{25°C}$ = 2.3–4.4), and metal concentrations (Table 1 and references therein). Black smoker chimney samples from the Main Endeavour Field include those collected prior to the seismic swarm and inferred tectonic/volcanic event that occurred in 1999 (Alv1931) and immediately following (Alv3474-3-1 and Alv3480-4; Johnson et al., 2000). This event led to changes in the temperature and composition (pH, chlorinity, dissolved H_2) of hydrothermal fluids venting at the Main Endeavour Field including a temporary increase in temperature and decreases in chlorinity and pH (Seewald et al., 2003; Seyfried et al., 2003; Lilley et al., 2003).

2.2.Hydrothermal Vent Fluids

This study additionally presents new data on the concentrations of trace elements in hydrothermal vent fluids from the Tahi Moana-1, ABE, Tu'i Malila, and Mariner vent fields sampled during cruises TN236 (2009, R/V Thompson) and RR1507 (2015, R/V Roger Revelle). These vent fields are located along the Eastern Lau Spreading Center (ELSC) and Valu Fa Ridge (VFR) back-arc spreading centers in the Lau Basin of the southwestern Pacific Ocean (Ferrini et al., 2008; Evans et al., 2017). Published data for fluids paired with black smoker chimney samples from the southern East Pacific Rise include temperature, pH, and major element concentrations, but do not include concentrations of Co, Ni, Ga, Ag, or In (O'Grady, 2001).

166 More comprehensive trace element data are available for vent fluids collected from the Main
167 Endeavour Field in 1999 (Co, Ni, and Ag; Seyfried et al., 2003), the Manus Basin in 2005 (Co
168 and Ag; Craddock, 2009), and the Beebe/Piccard vent field in 2012 (Co; McDermott et al., 2018).
169
170 3. METHODS
171 3.1. Hydrothermal Vent Fluids
172 3.1.1. Sample Collection and Shipboard Analyses
173 Hydrothermal vent fluids from the actively venting Tahi Moana-1, ABE, Tu'i Malila and
174 Mariner vent fields were collected using the remotely operated vehicle, *Jason II*. One to three
175 fluid samples from each vent were collected in 150 mL isobaric gas-tight (IGT) samplers
176 (Seewald et al., 2002). Vent fluid temperatures were measured using a thermocouple mounted on
177 the inlet snorkel of the IGT sampler. Following shipboard recovery, fluid samples were analyzed
178 for pH at room temperature using a Ag/AgCl combination reference electrode that was calibrated
179 daily. Aliquots for major element- and trace metal analyses were transferred to acid-washed
180 high-density polyethylene (HDPE) Nalgene™ bottles and aliquots for trace metal analysis were
181 acidified with analytical-grade Optima™ HCl prior to storage. In many fluid samples a
182 precipitate "dregs" fraction formed upon initial collection and cooling of the sample. This was
183 recovered from the inside of the IGT sampling bottle by rinsing with Milli-Q filtered water and
184 high-purity acetone; precipitates were collected on 0.22 μm pore-size, 44 mm diameter Nylon
185 filters.
186
187 3.1.2. Digestion of Dregs and Filter Fractions

188 Aliquots of hydrothermal fluid samples for minor and trace element analysis by ICP-MS
189 were filtered into HDPE Nalgene™ bottles through 0.22 μm pore-size, 22 mm diameter
190 Nuclepore® nylon filters to remove additional precipitates (a.k.a. the "filter" fraction) that might
191 have formed during storage. Syringes, filters, filter units, and fluid handling equipment were all
192 acid-cleaned with 0.8 M HNO_3 prepared from analytical grade Optima® HNO_3 (Thermo Fisher
193 Scientific, Agawam, MA) and Milli-Q filtered water. Visible particles sticking to the sides of
194 laboratory vessels were transferred with the aid of Milli-Q filtered water and high-purity ethanol.
195 Precipitate filter and dregs fractions were then digested in reverse *aqua regia* (three parts 16 M
196 analytical grade Optima® HNO_3 to 1 part 12 M analytical grade Optima® HCl by volume) in
197 Savillex™ digestion vials and left at 70°C until dry. Samples were then brought up in 5 mL of
198 0.8 M HNO_3 and left to dry a second time to remove any remaining HCl. Finally, these samples
199 were brought up in 30 mL 0.8 M HNO_3 and stored in HDPE Nalgene® bottles prior to analysis.
200
201 3.1.3. Major and Trace Element Analysis
202 Analyses of major elements (Na, K, Li, Ca, Mg) were conducted on diluted samples of
203 dissolved aliquots of hydrothermal fluids by ion chromatography at WHOI. Analyses of minor
204 elements (Fe, Mn) and trace elements (Cr, Co, Ni, Cu, Zn, Ga, Rb, Mo, Ag, Cd, In, Sn, Cs, Au,
205 and Pb) were carried out on diluted samples of "dissolved" fractions and digested "filter" and
206 "dregs" fractions using the Element 2 inductively coupled plasma mass spectrometer at the
207 Plasma Mass Spectrometry Facility at WHOI.
208 To calculate the metal concentrations of the initial hydrothermal fluid venting at the
209 seafloor, the separate contributions of the dregs-, filter-, and dissolved fractions were summed.
210 Data were then extrapolated from the composition of local seawater to an endmember

hydrothermal composition containing zero-Mg (Von Damm et al., 1985; Trefry et al., 1994; Metz and Trefry, 2000). While this method is generally effective, significant uncertainties arise when mineral deposit particles care inadvertently entrained during vent fluid sampling. Furthermore, recovery of dregs- and filter fractions can be incomplete. If multiple fluid samples have been taken from the same vent, then the quality of fluid sampling can be confirmed if multiple samples extrapolate to similar zero-Mg endmember concentrations. Alternatively, likely sampling artifacts can be identified if multiple samples extrapolate to extremely different endmember compositions. In some cases, the likely quality of fluid sampling can also be inferred by comparison with replicate samples from the same vent field that exhibit similar temperature, pH, chlorinity, etc. However, if only one fluid sample has been taken from a given vent, the quality of fluid sampling cannot be definitively determined.

3.2. Black Smoker Chimney Linings

3.2.1. Sample Collection and Preparation

Black smoker chimney samples were collected from active seafloor vent fields using the manipulator grab arms of the remotely operated vehicle, *Jason II,* or the human occupied vehicles *Alvin* or *Nautile*. SMS deposit samples were photographed and air-dried following shipboard recovery and transferred to climate-controlled storage upon arrival at WHOI.

3.2.2. Electron Microprobe Analysis

Electron microprobe analyses of black smoker chimney linings were conducted using the JEOL JXA-8200 at the Massachusetts Institute of Technology Electron Microprobe Facility. Analyzed spots were located along the innermost edges of black smoker chimneys adjacent to

234 fluid conduits in areas free of visible inclusions and preferably next to the circular pits left by
235 SIMS analyses. Concentrations of Cu, Fe, and S were calibrated against an in-house chalcopyrite
236 ($CuFeS_2$) reference material. Count times were 40 s for each element. As evaluated by multiple
237 measurements on the same sample, measurement precision is ~0.5 wt%. Mass totals of accepted
238 analyses are between 99 wt% and 101 wt%. Analyses of Co, Ni, and Ag were also attempted.
239 However, concentrations of these elements are generally below detection limits and do not offer
240 quantitative analyses.
241
242 3.2.3 Secondary Ion Mass Spectrometry (SIMS)
243 In preparation for SIMS analysis, black smoker chimney samples were cut, mounted in
244 epoxy, polished to 1 μm grit with diamond and/or alumina abrasives, and gold coated. Trace
245 element analyses were obtained using the Cameca IMS 1280 ion microprobe at the Northeast
246 National Ion Microprobe Facility at WHOI. Secondary ion intensities were measured for $^{59}Co^+$,
247 $^{60}Ni^+$, $^{69}Ga^+$, $^{109}Ag^+$, $^{113}In^+$, and $^{115}In^+$. Secondary ion intensities of trace elements are reported as
248 a ratio against the secondary ion intensity of $^{63}Cu^{16}O^+$, which was found to be more stable than
249 that of $^{54}Fe^{16}O^+$. Measurements of $^{75}As^+$ and $^{74}Ge^+$ were also attempted. However, $^{75}As^+$ was
250 found to be heterogeneous in chalcopyrite and ion intensities for $^{74}Ge^+$ were below detection
251 limits in all black smoker chimney samples investigated.
252 Spot sizes of ~40 μm enabled analyses of the innermost linings of black smoker
253 chimneys, including samples with finely intergrown chalcopyrite and wurtzite or chalcopyrite
254 and pyrite. A typical mass resolving power of ~10,000 enabled adequate peak separation (Fig. 2).
255 Detection limits were set at three standard deviations above the mean ion intensity measured on
256 background mass 54.7. This was evaluated to be 0.25 counts per second (cps) or 5×10^{-5} cps / cps

257 $^{63}Cu^{16}O^{+}$. Quantitative determination limits were set at ten standard deviations above the mean
258 secondary ion intensity measured on the background mass 54.7. This was evaluated to be 0.6 cps
259 or 1.2×10^{-4} cps / cps $^{63}Cu^{16}O^{+}$. Machine settings, typical secondary ion intensities and associated
260 errors for $^{63}Cu^{16}O^{+}$, detection limits, and determination limits are listed in Table 2.
261 To monitor for possible wurtzite/sphalerite and/or pyrite inclusions, intensities on masses
262 corresponding to $^{54}Fe^{16}O^{+}$ and $^{64}Zn^{16}O^{+}$ were also measured. Likely sputtering of mineral
263 inclusions was particularly notable in black smoker chimney linings composed of intergrown
264 chalcopyrite and wurtzite. Accordingly, spots with anomalously high $^{64}Zn^{16}O^{+}$ intensities and
265 correspondingly low $^{63}Cu^{16}O^{+}$ intensities were removed from the dataset prior to statistical
266 analysis. For each black smoker chimney sample, sample means and standard errors were
267 calculated over the total number of measurements on that sample in each analytical session.
268 Reported trace element ratios obtained during different sessions were then reconciled by
269 reference to common samples analyzed during multiple sessions. During each session, black
270 smoker chimney samples shown to be homogeneous with respect to several of the trace elements
271 of interest were used as provisional reference materials to monitor machine stability using the
272 sample-standard bracketing method (typically five sample spots bracketed by two standard spots).
273 The standard error of secondary ion ratios measured on these provisional reference materials was
274 typically < 15% of the mean secondary ion ratio.
275 Additional statistical modeling of SIMS results in the construction of calibration curves
276 and subsequent comparisons with fluid or mineral parameters were carried with Microsoft Excel
277 software using the LINEST and other appropriate functions. The number of samples (n) was
278 taken to be the total number of SIMS spot analyses. The number of distinct sample averages (c)
279 was taken to be the total number of black smoker chimney linings included in each comparison.

280

281 3.2.4. Digestion and ICP-MS Analysis of Picked Chalcopyrite Grains

282 To generate SIMS calibration curves, chalcopyrite from a subset of the black smoker
283 chimney linings analyzed by SIMS was picked for total acid digestion and analysis by ICP-MS
284 against NIST-traceable reference solutions. Picked grains were obtained from the innermost
285 linings of black smoker chimneys within 1 mm of the main fluid conduit by coarse crushing with
286 an agate motor and pestle followed by careful picking with non-metal tools. Sample grains were
287 then individually examined under a Leica Stereo Zoom 6 Photo microscope and transferred to a
288 separate container in order to ensure minimally tarnished samples of purest possible chalcopyrite.
289 Additionally, polished sections of the same samples were examined under a reflected light
290 petrographic microscope to ensure that samples in this subset did not contain visible inclusions
291 of other minerals along the chimney lining.

292 Samples of picked chalcopyrite grains were weighed to a precision of ~ 0.05 mg before
293 being digested in reverse *aqua regia* (1 part 12 M HCl : 3 parts 16 M HNO_3, by volume) in acid-
294 cleaned Savilllex digestion vials and diluted in 30 mL of 0.8 M HNO_3 before being transferred to
295 Teflon-coated bottles. Sample solutions were then prepared for measurement by ICP-MS by
296 further diluting aliquots of the 30 mL sample dilutions with 0.8 M HNO_3 containing 1 ng/g Sc
297 and 1ng/g Y as internal spikes to a target strength of 2 μg/g Cu for trace element analyses and a
298 target strength of 50 ng/g Cu for major element analyses.

299 Major and trace element analyses of digested chalcopyrite (and cubanite) picks were
300 obtained using the Element 2 (Thermo Fisher Scientific, Waltham, USA) at the Plasma Mass
301 Spectrometry Facility at WHOI. ICP-MS analyses were calibrated against serial dilutions of
302 Specpure® plasma solutions with 0.8 M HNO_3 containing 1 ng/g Sc and 1 ng/g Y as internal

303 spikes. Relative errors of the analysis were estimated by repeat measurements of the same
304 sample solution and are generally on the order of 10%.
305
306 3.3. Thermodynamic Modelling of Aqueous Complexing
307 To compare the measured trace element chemistry of black smoker chimney linings with
308 the hydrothermal fluid chemistry at *in situ* temperatures and pressures present at the seafloor, the
309 activities of aqueous complexes and free ions were calculated using the EQ3/6 software package
310 (Wolery, 1992) and thermodynamic data compiled in the SUPCRT92 database (Johnson et al.,
311 1992) modified as described by Tivey et al. (1999) and Tivey (2004), which include the Fe-Cl
312 complex data of Ding and Seyfreid (1992). Thermodynamic data for Co, Ni, and In chloride
313 complexes and Ga and In hydroxide complexes were obtained from the SLOP07 database
314 available at http://geopig3.la.asu.edu:8080/GEOPIG pigopt1.html (Shock et al., 1997;
315 Sverjensky et al., 1997). Model inputs are presented in Table 3. The dissociation reaction
316 constants for selected complexes at various temperatures are listed in Supplementary Table S1.
317 Of particular interest for the comparison between black smoker chimney linings and
318 hydrothermal vent fluids is the calculation of *in situ* pH, which may be several pH units above
319 shipboard measurements conducted at 25°C. In contrast, calculations of *in situ* pH have been
320 shown to be within 0.1–0.4 units of *in situ* measurements of vent fluid pH conducted at the
321 seafloor, suggesting that these thermodynamic calculations lead to a close approximation of
322 actual *in situ* pH (Ding et al., 2005).
323
324 4. RESULTS
325 4.1. Trace Elements Concentrations in Black Smoker Chimney Linings

326 A total of 29 black smoker chimney samples were analyzed for Co, Ag, and In using
327 SIMS of which 22 were additionally analyzed for Ni and Ga. To generate calibration curves and
328 quantify SIMS measurements picked chalcopyrite grains from five of these samples were
329 analyzed by ICP-MS. The stoichiometry of 14 of these samples was determined using electron
330 microprobe analysis. Trace element analyses obtained by SIMS are reported as secondary ion
331 ratios (Table 4) and absolute concentrations (Table 5) based on calibration curves obtained by
332 comparing SIMS and ICP-MS results (Fig. 3).
333
334 4.1.1. Evaluation of SIMS Calibration Curves
335 Trace element calibration curves were constructed based on analyses of selected black
336 smoker chimney samples by SIMS and solution ICP-MS calibrated against NIST-traceable
337 solution standards (Fig. 3). These samples are characterized by monomineralic linings,
338 reproducible SIMS measurements, and untarnished (or mildly tarnished) grains of picked
339 chalcopyrite. Total sample recovery based on ICP-MS analyses of major elements in grains of
340 chalcopyrite picked from the innermost linings of black smoker chimneys range from 86 ± 6 wt%
341 to 108 ± 5 wt% with the exception of one sample with 63 ± 3 wt % total recovery (Table 5).
342 Concentrations of Zn, Ca, Ba, and Si account for less than 0.3 wt% of this sample, suggesting
343 that the gap in total recovery cannot be explained by contamination with other common SMS
344 deposit minerals (e.g., sphalerite/wurtzite, anhydrite, barite, amorphous silica; Table 6).
345 Following the assumption that differences in mass balance are primarily caused by the inefficient
346 or unrecorded transfer of small sample grains between different laboratory containers, reported
347 major and trace element mass fractions have been normalized to 100% recovery.

In general, concentrations of trace elements are consistent between different picks of the same sample and different digestions of the same pick (Table 6). In contrast, concentrations of trace elements vary widely between samples of different black smoker chimneys, both within a given vent field and between different vent fields. Ranges of trace element concentrations in picked grains of chalcopyrite analyzed by solution ICP-MS are (Table 7): Co (0.3 μg/g – 150 μg/g), Ni (30 μg/g – 1120 μg/g), Ga (0.3 μg/g – 40.4 μg/g), Ag (100 μg/g – 2900 μg/g), In (5.9 μg/g – 77 μg/g). High background counts of 400 – 670 cps for Ni^{60} in ICP-MS analyses, possibly an artifact of Ni cones used in the Element 2, mean that only two samples, Alv3299-6-1 and Alv3296-3, can be accurately analyzed for Ni by ICP-MS. However, these two samples are sufficient to construct adequate calibration curves. Moreover, SIMS analyses are not affected and high-quality measurements of Ni in black smoker chimney linings can be achieved with low detection limits.

Based on the combined ICP-MS and SIMS analyses, suitable calibration curves for Co, Ni, and Ag can be drawn for the full range of concentrations exhibited by the black smoker chimney linings investigated in this study (Fig. 3). Calibration curves can also be drawn for Ga and In, albeit within a limited concentration range (Fig. 3). Uncertainties in the slopes of the calibration curves based on calculated 95% confidence intervals are: Co (6.5%), Ni (10.9%), Ga (5.4%), Ag (9.9%), and In (22.0%).

For Ga and In, reasonably precise calibration curves are achieved between the concentrations of 0 – 10 μg/g for Ga and 0 – 40 μg/g for In. A main factor that may affect the quality of SIMS calibration curves is the extent of trace element homogeneity at mm- to cm-scales. Small amounts of zinc sulfide contamination in aliquots of picked chalcopyrite grains could explain the uncertainty of the Ga and In calibration curves at higher concentrations.

However, arguments against this explaniation include a lack of significant correlations between Zn and any of these elements in ICP-MS analyses of picked grains and an absense of intergrown wurtzite or sphalerite observed under the petrographic microscope. Alternatively, Ga and In could be less homogeneously distributed in chalcopyrite chimney linings than Co, Ni, and Ag. This explanation is supported by SIMS analyses where the relative standard errors over multiple spots are typically greater for Ga and In than for Co, Ni, and Ag.

4.1.2. SIMS Analyses of Trace Elements Concentrations in Black Smoker Chimney Linings

The concentrations of trace elements in black smoker chimney linings based on SIMS measurements and calibration curves cover the following ranges: Co (< 2 ng/g to 760 μg/g), Ni (< 17 ng/g to 454 μg/g), Ga (< 0.9 ng/g to 48 μg/g), Ag (60 μg/g to 3800 μg/g), In (<0.5 ng/g to 270 μg/g) (Table 5). For the purposes of this paper, the abundance and homogeneity of trace elements in each black smoker chimney lining is approximated by the mean and standard errors (1σ) of all SIMS measurements obtained on that sample. Reported uncertainties of trace element concentrations reflect only the uncertainties derived from multiple SIMS analysis and do not reflect the additional uncertainties associated with the slopes of the calibration curves. The reasoning behind this presentation is to maintain focus on the extent of natural variability of trace element concentrations within each sample rather than propagating the uncertainties of the calibration curves discussed in section 4.1.1.

In general, the variability of trace element concentrations between samples of black smoker chimney linings is larger than the variability within a single sample. Arranged in descending order, concentrations of Co and Ni are: Mid-Cayman Rise > southern East Pacific Rise ~ Main Endeavour Field (post-event) > SuSu Knolls > PACMANUS ~ Eastern Manus Basin ~ Main Endeavour Field (pre-event) ~ Valu Fa Ridge ~ Eastern Lau Spreading Center.

Concentrations of Co and Ni are typically higher in black smoker chimney samples from basalt-hosted vent fields than in those from felsic-hosted back-arc vent fields in the Lau and Manus Basins with the exception of samples from SuSu Knolls, which exhibit intermediate Co and Ni concentrations (Fig. 4). Additionally, the log concentrations of Co and Ni covary ($\log_{10}$(Co) vs. $\log_{10}$(Ni): $R^2 = 0.85$; $p < 0.0001$) in basalt-hosted and SuSu Knolls samples, with the highest concentrations of both Co and Ni present in sample J2-613-16-R1 from the Beebe/Piccard vent field on the Mid-Cayman Rise (Fig. 4). Concentrations of Co and Ni in samples from felsic-hosted systems other than SuSu Knolls are low and do not covary. Concentrations of Ga are higher in black smoker chimney linings from felsic-hosted vent systems, while Ag and In exhibit no obvious association with the lithology of host rocks or geologic settings. The log concentration of Ga and In weakly covary ($\log_{10}$(Ga) vs. $\log_{10}$(In): $R^2 = 0.37$, $p = 0.0056$).

The homogeneity of trace elements in black smoker chimney linings was evaluated by calculating the standard error of the SIMS count ratios, reported as a percentage of the mean secondary ion ratio. The extent of trace element homogeneity varies widely between samples. However, relative standard errors (1σ) for the majority of samples lie between 5% and 25% for Co, Ni, and Ag and between 5% and 50% for Ga and In. The median relative standard errors for all black smoker chimney samples examined in this study are: Co (40%), Ni (14%), Ga (29%), Ag (24%), and In (35%). For Co, relative standard errors negatively correlate with Co concentration. If only the 12 samples containing > 1 μg/g Co are considered, the median relative standard error for Co is reduced to 13%. The relative standard errors of other trace elements do not correlate with concentration.

4.1.3. Stoichiometry of Black Smoker Chimney Linings

418 The stoichiometry of 14 of the black smoker chimney linings analyzed by SIMS was
419 analyzed by electron microprobe. The molar ratios of Cu:Fe for all but two of these samples are
420 equivalent to chalcopyrite within error (i.e., 0.95 < Cu:Fe < 1.01). Exceptions include sample
421 Alv3299-6-1 from the southern East Pacific Rise with a Cu:Fe molar ratio of 0.93 and sample J2-
422 613-16-R1 from the Beebe/Piccard vent field on the Mid-Cayman Rise with a Cu:Fe molar ratio
423 of 0.65.
424 The Cu:Fe molar ratios of samples evaluated by electron microprobe correlate with
425 concentrations of Co and Ni (R^2 = 0.97 for Cu:Fe vs. Co; R^2 = 0.98 for Cu:Fe vs. Ni, Fig. 5).
426 While regression lines and correlation coefficients are strongly controlled by sample J2-613-16-
427 R1, correlation coefficients calculated without including this sample remain statistically
428 significant (Cu:Fe vs. Co: R^2 = 0.55, p = 0.0035; Cu:Fe vs. Ni: R^2 = 0.73, p = 0.0004) and lack-
429 of-fit calculations indicate that linear regression models can appropriately fit the data.
430
431 4.2. Hydrothermal Vent Fluids
432 A total of 60 hydrothermal vent fluid samples were collected from 33 active vents (12 in
433 2009 and 21 in 2015) at the Tahi Moana-1, ABE, Tu'i Malila, and Mariner vent fields. Of these
434 samples, 45 contained < 10 mmol/kg Mg, indicative of low extents of seawater entrainment prior
435 to or during sampling (< 20% seawater by mass). Reported ranges of endmember fluid
436 concentrations are based on reproducible duplicate samples obtained from 27 of the 33 vents. A
437 full report of calculated zero-Mg endmember compositions of low-Mg vent fluids is presented in
438 Table 8. Additionally, Supplementary Tables S2 – S5 contain the separate contributions of the
439 dissolved-, filter-, and dregs fractions and the total concentrations of analyzed elements in these
440 fluids prior to calculation of the zero-Mg endmember values.

441 The temperature, $pH_{25°C}$, and zero-Mg endmember concentrations of major ions (Na, Li,
442 K, Ca) of vent fluids examined in this study have been reported in Seewald (2017).
443 Concentrations of Mn, Fe, Cu, Zn, Co, Ni, Ga, and Ag are available for ELSC/VFR vent fluids
444 collected in 2009 and 2015, while concentrations of In are only available for vent fluids from the
445 ABE, Tu'i Malila, and Mariner vent fields collected in 2015. No significant difference in vent
446 fluid concentrations is observed between samples collected in 2009 and those collected in 2015.
447
448 4.2.1. Mn, Fe, Cu, Zn, and Cd
449 Ranges in endmember fluid concentrations for Mn, Fe, Cu, Zn and Cd are: Mn (240 ± 27
450 μmol/kg – 6,090 ± 50 μmol/kg), Fe (48 ± 3 μmol/kg – 14,000 ± 300 μmol/kg), Cu (4 ± 1
451 μmol/kg – 300 ± 16 μmol/kg), Zn (37 ± 1 μmol/kg – 1,800 ± 100 μmol/kg), Cd (54 ± 4 nmol/kg
452 – 1,5600 ± 40 nmol/kg). Metal concentrations are typically greater in the higher-temperature
453 (308–364°C), lower-pH ($pH_{25°C}$ = 2.2–2.7) fluids collected from the Mariner vent field than in
454 the lower-temperature (232–317°C), higher-pH ($pH_{25°C}$ = 3.7–4.5) vent fluids collected from the
455 Tahi Moana-1, ABE, and Tu'i Malila vent fields (Fig. 6). Likewise, endmember Zn and Cd
456 concentrations show similar levels of enrichment in the lower-pH, higher-temperature vent fluids
457 from the Mariner vent field relative to fluids from higher-pH, lower-temperature vent fluids from
458 other ELSC/VFR vent fields (Table 7; Fig. 6). However, some overlap occurs between Zn-rich
459 vent fluid samples from the Tu'i Malila vent field and Zn-poor vent fluid samples from the
460 Mariner vent field.
461
462 4.2.2. Co, Ni, Ga, Ag, and In

463 Relative to measurements of Mn, Fe, Cu, Zn, and Cd, measurements of Co, Ni, Ga, Ag,
464 and In in hydrothermal vent fluids are more sparse and less precise. This can be attributed to the
465 lower concentrations of these elements and the importance of the dregs fraction in determining
466 concentrations of these elements. Dregs fractions are less routinely measured than dissolved
467 fractions and are more likely to be incompletely recovered and/or affected by contamination with
468 deposit minerals. Nevertheless, reproducible measurements of trace metals, including Co, Ni, Ga,
469 Ag, and In were achieved (Table 7). Ranges of endmember fluid concentrations are: Co (73 ± 1
470 nmol/kg – 500 ± 130 nmol/kg), Ni, (76 ± 3 nmol/kg – 1,100 ± 600 nmol/kg), Ga (2 ± 0 nmol/kg
471 – 280 ± 28 nmol/kg), Ag (2 ± 1 nmol/kg – 100 ± 14 nmol/kg), and In (40 ± 4 nmol/kg – 240 ± 50
472 nmol/kg).
473 Endmember Co concentrations are 1–4× greater in Mariner vent fluids than in other
474 ELSC/VFR vent fluids (Table 7; Fig. 7). Gallium concentrations are 1–5× greater in vent fluids
475 from the Mariner vent field than in vent fluids from the ABE and Tu'i Malila vent field, which
476 are in turn greater than Ga concentrations in vent fluids from the Tahi Moana-1 vent field (Table
477 7; Fig. 7). Relatively fewer reproducible measurements were obtained for Ni and Ag, inhibiting
478 a definitive comparison between vent fields. However, endmember Ni concentrations are highest
479 in fluids from the Mariner vent field while concentrations of Ag in Mariner vent fluids lie within
480 the range of concentrations exhibited by other vent fields (Table 7, Fig. 7).
481 Because In was used as an internal spike during ICP-MS analyses of fluids collected in
482 2009 and in analyses of all dissolved fractions, analyses of In are only available for the dregs and
483 filter fractions of fluids collected in 2015. Based on these data, endmember In concentrations are
484 approximately 2–4× greater in vent fluids collected from the Mariner vent field than in vent

485 fluids from the ABE and Tu'i Malila vent fields (Table 7; Fig. 7). In was not analyzed in Tahi
486 Moana-1 vent fluids, which were collected in 2009.
487
488 5. DISCUSSION
489 5.1. Incorporation of Trace Elements into Black Smoker Chimney Linings
490 Results of optical microscopy and electron microprobe analyses indicate that the black
491 smoker chimney linings investigated in this study are composed of chalcopyrite ($CuFeS_2$) or Cu-
492 Fe-S intermediate solid solutions that are chemically intermediate between chalcopyrite and
493 cubanite ($CuFe_2S_3$). Based on analyses of X-ray synchrotron and Mössbauer spectral data, Pearce
494 et al. (2006) conclude that the crystal chemistry of chalcopyrite is best modelled as
495 $Cu(I)Fe(III)S(-II)_2$. Similarly, analysis of Mössbauer spectra by Greenwood and Whitfield (1968)
496 and subsequent analysis of X-ray synchrotron data by Goh et al. (2006) lead these authors to
497 conclude that the crystal chemistry of cubanite is best modelled as $Cu(I)Fe(II)Fe(III)S(-II)_3$.
498 Of the various trace elements investigated in this study, Ag and In have been previously
499 proposed to occur as lattice substitutions in chalcopyrite (Ag(I) for Cu(I) and In(III) for Fe(III);
500 Huston et al., 1995). This determination was based on four criteria: (1) the crystal chemistry of
501 the host mineral, (2) experimental studies on the solubilities of the elements of interest in the
502 host mineral, (3) the presence or absence of minerals that contain major concentrations of the
503 elements of interest (e.g., Lenaite ($AgFeS_2$) and Roquesite ($CuInS_2$)), and (4) variations in the
504 concentrations of the elements of interest between and within samples (Huston et al., 1995).
505 Extending this logic to the SIMS analyses of trace elements in black smoker chimney linings
506 presented here, it is likely that Co, Ni, and Ga also exist as lattice substitutions in chalcopyrite.

Based on shared valence state and the existence of gallite ($CuGaS_2$), Ga(III) is proposed to substitute for Fe(III) in the chalcopyrite crystal lattice. The reproducibility of SIMS data for Co and Ni in chalcopyrite and Cu-Fe-S solid solutions lining black smoker chimneys similarly suggests that these elements are present as lattice substitutions. However, the low concentrations of these elements in chalcopyrite and correlation between Co and Ni concentrations and the Cu:Fe molar ratio of Cu-Fe-S solid solutions suggest that these elements preferentially substitute for the Fe(II) site present in more Fe-rich intermediate solid solutions (Fig. 5). Previous studies have likewise reported the presence of high Co concentrations in Fe-rich intermediate solid solutions (e.g., $CuFe_2S_3$, $CuFe_3S_4$, Rouxel et al., 2004).

5.2. Effects of Hydrothermal Fluid Chemistry on Mineral Trace Element Concentrations

This study focuses on the chemistry of black smoker chimney linings formed in direct contact with venting hydrothermal fluids under well-constrained physiochemical conditions. Thus, concentrations of Co, Ni, Ga, Ag, and In measured by SIMS may be directly compared with the temperature and chemistry of venting hydrothermal fluids, presented here or in previous studies (Seyfried, 2003; Craddock, 2009; Reeves et al., 2011; Mottl et al., 2011; Seewald, 2017; Evans et al., 2017; McDermott et al., 2018).

This study does not address the chemistry of minerals formed within the chimney wall, for which the relevant physiochemical parameters are less certain (e.g., Tivey, 1995). Moreover, this study centers attention on black smoker chimney linings that exhibit spatial homogeneity with respect to Co, Ni, Ga, Ag, and In and are thus most likely to reflect the physiochemical parameters of sampled vent fluids. Detailed investigation of trace element distributions in

529 samples exhibiting spatial heterogeneity (e.g., Ag in J2-213-6-R1) and possible connections with
530 spatio-temporal varability in venting hydrothermal fluids remains for future study.
531
532 5.2.1. Trace Element Partitioning of Ag

533 The incorporation of Ag(I) derived from the fluid as a trace element substituting for Cu(I)
534 in chalcopyrite lining a black smoker chimney may be represented by the following ion exchange
535 reaction:

536 $$Ag^+ + CuFeS_{2\,(s)} \leftrightarrow Cu^+ + AgFeS_{2\,(s)} \quad (1)$$

537 where $AgFeS_{2\,(s)}$ and $CuFeS_{2\,(s)}$represent endmember components in a Ag-containing
538 chalcopyrite solid solution. Based on the above chemical reaction, the following mass action
539 expression may be written:

540 $$K_{eq} = \frac{\{Cu^+\}\{AgFeS_{2\,(s)}\}}{\{Ag^+\}\{CuFeS_{2\,(s)}\}} \quad (2)$$

541 where K_{eq} is the equilibrium constant for reaction 1. Because trace levels of $AgFeS_2$ are present
542 in chalcopyrite solid solutions examined during this study, the mole fraction and activity of
543 $CuFe_{2(s)}$ can be assumed to be unity. The activities of Ag^+ and Cu^+ in the corresponding
544 hydrothermal fluids may be calculated from the temperature, major element chemistry, and
545 measured concentrations of Ag and Cu using EQ3/6 and the vent fluid compositions listed in
546 Table 3. The ability to calculate thermodynamic activities at *in situ* temperatures and pressures is
547 necessary because the activity of Ag^+ and Cu^+ in hydrothermal fluids is largely controlled by the
548 formation of Cl^-, and HS^- complexes, a phenomenon that becomes more important at higher
549 temperatures.

550 To more directly consider the measured concentrations of Ag in black smoker chimney
551 linings rather than the unmeasured thermodynamic activities, the equilibrium reaction equation
552 may be rewritten:

553 $$K_{eq} = \frac{X_{\mathrm{AgFeS2}}\gamma_R}{\{\mathrm{Ag^+}\}/\{\mathrm{Cu^+}\}} \quad (3)$$

554 where X_{AgFeS2} is the mole fraction of $AgFeS_2$ in the solid and γ_R is an unknown Raoult's activity
555 coefficient that relates the mole fraction of $AgFeS_2$ in chalcopyrite to its thermodynamic activity.

556 Based on measured data, the molar concentration ratio of Ag:Cu in chalcopyrite lining
557 black smoker chimneys is significantly correlated with the molar concentration ratio of Ag:Cu in
558 the corresponding hydrothermal vent fluids ($R^2 = 0.89$, $p < 0.0001$), and with the free ion activity
559 ratio of $\{Ag^+\}:\{Cu^+\}$ ($R^2 = 0.91$, $p < 0.0001$; Fig. 8). Following the equations outlined above, the
560 slope of the best-fit line represents the value $\frac{K_{eq}}{\gamma_R}$, which is equal to 0.67 ± 0.12. Overall, these
561 correlations suggest that the concentration of Ag in chalcopyrite lining black smoker chimneys
562 records the activity ratios of $\{Ag^+\}:\{Cu^+\}$ that, because aqueous complexing of Ag^+ and Cu^+ are
563 similar, record the ratio of Ag:Cu in the corresponding hydrothermal fluids.

564 A potentially more practical, but less precise method of describing the distribution of
565 trace elements between two different phases assumed to be in thermodynamic equilibrium is the
566 partition coefficient, defined by the following equation (McIntire, 1963):

567 $$D = \left(\frac{Tr}{Cr}\right)_S / \left(\frac{Tr}{Cr}\right)_L \quad (4)$$

where D is the partition coefficient, $\left(\frac{Tr}{Cr}\right)_S$ is the ratio of the concentration of the trace element to that of the major or "carrier" element in the solid and $\left(\frac{Tr}{Cr}\right)_L$ is the ratio of the concentration of the trace element to that of the major element in the liquid or aqueous phase (McIntire, 1963). The partition coefficient, D, for the trace element substitution of Ag into chalcopyrite can be calculated with the following equation:

$$D = \frac{[\mathrm{Cu^+}]X_{AgFeS2(s)}}{[\mathrm{Ag^+}]X_{CuFeS2(s)}} \quad (5)$$

Equation 5 is analogous to Equation 2, but differs by the use of concentrations rather than thermodynamic activities. Unlike the value $\frac{K_{eq}}{\gamma_R}$, the partition coefficient does not take into account the effects of aqueous complexing, which are related to the chemistry and composition of the hydrothermal fluid. However, the calculated partition coefficient based on concentrations alone is 0.67±0.14, which is the same value as $\frac{K_{eq}}{\gamma_R}$,, within error.

That the Ag concentrations of chalcopyrite in black smoker chimney linings primarily reflect the Ag:Cu concentration ratios of corresponding hydrothermal vent fluids supports recent work indicating that the stoichiometry and stability of Cl^- and HS^- complexes with Ag^+ are similar to those of Cu^+ over a wide range of physiochemical conditions relevant to black smoker chimneys (Akinfiev and Zotov, 2001; Pokrovski, 2013). Unfortunately, the SLOP07 database does not include data on Cu bisulfide complexes, which are potentially important in controlling the activity of $\{Cu^+\}$ in sulfur-rich hydrothermal fluids. Follow-up investigations that include more explicit modeling of the Cl^- and HS^- complexes of both Ag^+ and Cu^+ in the fluids presented here would be valuable in providing a clearer understanding of the potential role of these complexes in controlling Ag and Cu concentrations in hydrothermal vent fluids.

With the exception of a few samples collected from the PACMANUS vent fields of the Manus Basin, the log concentrations of Ag in black smoker chimney linings also correlate with hydrothermal fluid pH (Fig. 9), either measured shipboard ($pH_{25°C}$ vs. $\log_{10}(Ag)$: $R^2 = 0.53$, $p = 0.003$), or as calculated for *in situ* conditions ($pH_{in\ situ}$ vs. $\log_{10}(Ag)$: $R^2 = 0.34$, $p = 0.027$). This pattern can be explained by partitioning of Ag into chalcopyrite as a function of the $\{Ag^+\}:\{Cu^+\}$ activity ratio in hydrothermal fluids and the effects of vent fluid pH on this ratio. Lower pH vent fluids, which result from higher reaction zone temperatures and/or the influence of acidic magmatic volatiles, contain higher Cu concentrations than less acidic vent fluids (Fig. S1). Because vent fluid Ag concentrations are observed to exhibit less sensitivity to differences in hydrothermal fluid pH relative to Cu, lower pH vent fluids have lower $\{Ag^+\}:\{Cu^+\}$ ratios than higher pH vent fluids (Fig. S1). Accordingly, chalcopyrite formed from lower pH vent fluids will tend to contain lower concentrations of Ag, reflecting the typically lower $\{Ag^+\}:\{Cu^+\}$ ratio. However, some low pH vent fluids contain very high concentrations of Ag, which has been attributed to remobilization of previously deposited Ag-rich metal sulfides in the subsurface (Craddock, 2009). In such cases, Ag concentrations in chalcopyrite lining black smoker chimneys are high, reflecting elevated $\{Ag^+\}:\{Cu^+\}$ ratios in the corresponding hydrothermal fluids (e.g., Fig. 8, sample J2-208-1-R1, pair with Fig. 9, sample RMR1). Thus, Ag-rich chalcopyrite in black smoker chimneys linings can either precipitate from higher-pH, Cu-poor vent fluids, or from Ag-rich low-pH vent fluids.

To differentiate between Ag-rich formed from higher-pH, Cu-poor vent fluids, and that formed from Ag-rich low-pH vent fluids, additional mineralogical or geochemical evidence may be necessary. For example, previous studies have shown that zonation of copper-iron- and zinc sulfides and strong correlations between concentrations of Ag and Zn in bulk samples are

612 indicative of formation from low-pH fluids (Tivey et al., 1999; Kristall et al., 2011; Evans et al.,
613 2017).
614
615 5.2.2. Concentrations of Ga and In: Indicators of Vent Fluid pH
616 On the basis of shared valence state, similar ionic radius, and the existence of the
617 minerals gallite ($CuGaS_2$) and lenaite ($CuInS_2$), Ga(III) and In(III) most likely substitute for
618 Fe(III) in the chalcopyrite crystal lattice. However, Ga and In concentrations in chalcopyrite
619 lining black smoker chimneys do not correlate with Ga and In concentrations of the
620 corresponding vent fluids, where measured, nor do they correlate with the calculated
621 $\{Ga^{3+}\}:\{Fe^{3+}\}$or $\{In^{3+}\}:\{Fe^{3+}\}$ ratios of these fluids, though data on Ga and In complexes at *in*
622 *situ* conditions are limited (Fig. S2).
623 Intriguingly, log concentrations of Ga and In in chalcopyrite lining black smoker
624 chimneys do correlate with the measured pH ($pH_{25°C}$ vs. $\log_{10}$(Ga): $R^2 = 0.51$, $p = 0.002$; $pH_{25°C}$
625 vs. $\log_{10}$(In): $R^2 = 0.53$, $p = 0.0009$) and calculated *in situ* pH for corresponding vent fluids (pH_{in}
626 $_{situ}$ vs. $\log_{10}$(Ga): $R^2 = 0.51$, $p = 0.002$; $pH_{in\ situ}$ vs. $\log_{10}$(In): $R^2 = 0.35$, $p = 0.01$). High Ga and In
627 concentrations in chalcopyrite black smoker chimney linings are associated with low-pH vent
628 fluids (Fig. 9). A possible explanation for the observed correlations is complexing of Ga and In
629 by OH^{-} at higher pH. Experimental investigations of Ga and In speciation as a function of pH
630 have indicated that the activities of free Ga^{3+} and In^{3+} are both lower at higher pH, a
631 phenomenon that has been attributed to the formation of Ga and In OH^{-} complexes (Wood and
632 Samson, 2006; Fig. 10). Thermodynamic modelling performed here likewise indicates that Ga is
633 predominantly complexed as $Ga(OH)^{+2}$ while In is primarily complexed as $InCl^{+2}$ and
634 secondarily as $In(OH)^{+2}$. In considering this hypothesis, it should also be noted that

635 thermodynamic data for the Cl^- and OH^- complexes of Ga^{3+} and In^{3+} are highly uncertain (Wood
636 and Samson, 2006). This uncertainty and the fact that few measurements of Ga and In in
637 hydrothermal fluids are available may explain the lack of correlation between calculated
638 $\{Ga^{3+}\}:\{Fe^{3+}\}$or $\{In^{3+}\}:\{Fe^{3+}\}$ ratios in hydrothermal fluids and the Ga and In concentrations of
639 chalcopyrite in corresponding black smoker chimney linings.
640 The observed correlations between the Ga and In concentrations in chalcopyrite lining
641 black smoker chimneys and hydrothermal fluid pH provide a useful empirical proxy of
642 hydrothermal fluid pH. When combined with Ag, the addition of Ga and In as indicators of
643 hydrothermal fluid pH allows for differentiation between Ag-rich chalcopyrite precipitated from
644 near-neutral, Cu-poor vent fluids and similarly Ag-rich chalcopyrite precipitated from lower-pH
645 Ag-rich vent fluids. Specifically, high Ag concentrations accompanied by low Ga and In
646 concentrations in chalcopyrite are indicative of precipitation from near-neutral, Cu-poor
647 hydrothermal fluids while high Ag, Ga, and In concentrations in chalcopyrite are indicative of
648 precipitation from low-pH, Ag-rich hydrothermal fluids, likely related to subsurface
649 remobilization of previously deposited Ag-rich sulfide deposits.
650
651 5.2.3. Co and Ni Concentrations More Strongly Reflect Crystallography

652 As with Ag, Ga, and In, concentrations of Co(II) and Ni(II) in black smoker chimney
653 linings likely reflect both substitution into the mineral lattice and concentrations in the vent fluid
654 relative to Fe(II). Concentrations of Co and Ni in black smoker chimney linings show no clear
655 correlations with total Co or Ni vent fluid concentrations, the free ion activities of these elements,
656 or the activity ratios of these elements to those of Cu or Fe in corresponding vent fluids. As
657 noted, concentrations of Co and Ni do correlate with the Cu:Fe ratio of the copper-iron-sulfide

host mineral (Fig. 5), which has also been noted in previous studies (Rouxel et al., 2004). This suggests that crystallography plays a significant role in determining the Co and Ni concentrations of black smoker chimney linings, and Co and Ni concentrations in the mineral are not related to fluid metal concentrations in as straightforward a manner as was observed for Ag, Ga, and In. Specifically, a molar excess of Fe over Cu increases the availability of Fe(II) lattice sites for which Co(II) and Ni(II) preferentially substitute.

Previous studies have noted that Fe-rich Cu-Fe –S solid solutions are associated with lower sulfidation states that are in turn associated with H_2-rich fluids generated by hydrothermal reactions involving mafic or ultramafic host rocks (Kojima and Sugaki, 1985; Sack and Ebel, 2006; Einaudi, 2006; Kawasumi and Chiba, 2017). Data presented here confirm that copper-iron sulfide black smoker chimney linings from mafic-hosted Mid-Cayman Rise and southern East Pacific Rise vent fields are generally more Fe-rich and contain higher Co and Ni concentrations than their back-arc basin counterparts (Fig. 5). However, even in chimneys lined solely with stoichiometric chalcopyrite, no correlations are observed between Co or Ni concentrations of the black smoker chimney linings and hydrothermal fluid chemistry (Fig. 11), likely reflecting a lack of availability of Fe(II) lattice sites for which Co(II) and Ni(II) can substitute and suggesting a possibility of paired substitutions. Thus, the Co and Ni concentrations of black smoker chimney linings have not been shown to provide effective proxies of hydrothermal fluid chemistry beyond existing mineralogical indicators (e.g., Lusk and Bray, 2002).

5.3. Concentrations of Trace Metals in ELSC/VFR Hydrothermal Fluids

679 Metal concentrations in hydrothermal fluids are initially set in high-temperature
680 hydrothermal reaction zones, where chemically evolved seawater reacts with rocks (± magmatic
681 volatiles) below the seafloor (e.g., Seewald and Seyfried, 1990). As hydrothermal fluids travel
682 upward from these subsurface reaction zones to vents at the seafloor, metal concentrations may
683 be additionally modified by the precipitation and dissolution of SMS deposits and other minerals.
684 The extent to which the concentration of an element is modified by mineral precipitation and
685 dissolution depends on the partitioning of that element between minerals and hydrothermal fluids
686 and the extent of mineral precipitation/dissolution relative to the flux of hydrothermal fluid.
687 Elements that occur as major or trace elements in chalcopyrite and other sulfide minerals may be
688 especially sensitive to the precipitation and remobilization of previously deposited sulfide
689 minerals.

690 The similarity of ELSC/VFR vent fluids collected in 2015 to those collected in 2009 and
691 2005 with respect to temperature, pH, and element concentrations suggests that vent fluid
692 temperatures and chemistry have remained relatively stable during this time period. Vent fluids
693 collected from the Mariner vent field exhibit a bimodal range of chlorinity and H_2S contents that
694 has been attributed to phase separation at the seafloor and in the shallow subsurface (Takai et al,
695 2008; Mottl et al., 2011). However, there is no indication of systematic changes in the
696 compositions of high chloride or low chloride vent fluids at the Mariner vent field between
697 repeat visits. Metal concentrations in the high-temperature, low-pH vent fluids collected from the
698 Mariner vent field are higher than those in lower-temperature, higher-pH vent fluids collected
699 from other ELSC/VFR vent fields (Fig. 6, 7; Table 8). The magnitude of this enrichment varies
700 by element with Fe and Cu exhibiting the greatest enrichment and Ag exhibiting the least.

701 Concentrations of Co, Ga, Zn, Cd, and In are also enriched in Mariner vent fluids, but to a lesser
702 extent than Fe and Cu (Fig. 7).
703 Endmember concentrations of Mn in hydrothermal vent fluids including those from the
704 ELSC/VFR exhibit a negative trend with hydrothermal fluid pH with the highest Mn values
705 predominantly associated with fluids of pH < 3 (Fig. S3). Endmember Mn concentrations do not
706 correlate with vent fluid exit temperatures (Fig. S3). These patterns are consistent with the
707 previously proposed hypothesis that Mn concentrations reflect the temperature, pH, and other
708 chemical conditions of the hydrothermal reaction zone, but are not significantly modified by
709 mineral precipitation during subsequent cooling as the minerals that precipitate do not contain
710 significant quantities of Mn (Seewald and Seyfried, 1990). Some relatively high-pH, high-Mn
711 vent fluids from the Mariner vent field reflect mixing with seawater, which buffers the pH of
712 hydrothermal fluids, but does not significantly alter endmember Mn concentrations. Relatively
713 low Mn concentrations in low-Cl fluids collected from the Juan du Fuca Ridge point to the
714 additional importance of Cl-complexing in controlling Mn concentrations (Seyfried et al., 2003).
715 Endmember concentrations of Fe and Cu in ELSC/VFR and other vent fluids exhibit a
716 negative trend with fluid pH and a positive trend with vent fluid exit temperatures (Fig. S3). This
717 is consistent with the hypothesis that Cu and Fe concentrations are controlled by the temperature-
718 and pH-dependent precipitation of sulfide minerals, including chalcopyrite (Seewald and
719 Seyfried, 1990). Measured concentrations of Cu in hydrothermal vent fluids show a greater
720 degree of variability than those of Fe. This can be accounted for by the greater sensitivity of Cu
721 measurements to mineral (e.g. chalcopyrite) precipitation during the collection of vent fluid
722 samples and the relatively high concentrations of Cu in the dregs and filter fractions that may not
723 have been quantitatively recovered during sample processing. Ratios of Cu to Fe in hydrothermal

724 fluids may be additionally affected by fluid redox and sulfidation states, though these patterns
725 may be obscured by temperature-dependent precipitation of chalcopyrite and associated removal
726 of Cu (Seyfried and Ding, 1993).

727 Endmember concentrations of Zn exhibit a negative trend with vent fluid pH and no trend
728 with respect to vent fluid exit temperatures (Fig. S3). This is consistent with experimental data
729 indicating that Zn concentrations initially set in the hydrothermal reaction zone equilibrate more
730 slowly than Cu and Fe during subsequent cooling (Seewald and Seyfried, 1990). An additional
731 factor may be the pH-dependence of sphalerite (ZnS) saturation temperatures, which causes Zn
732 to be precipitated at higher temperatures under higher pH conditions (Evans et al., 2017). Several
733 vent fluids from the relatively high pH Tu'i Malila vent field are enriched in Zn compared to the
734 other vent fluids (Fig. S3). Previous studies of hydrothermal vent fluids from the Vai Lili vent
735 field on the VFR (Fouquet et al., 1993), the TAG hydrothermal mound on the Mid-Atlantic
736 Ridge (Tivey et al., 1995; Metz and Trefry, 2000), and the PACMANUS vent fields in the
737 Manus Basin (Craddock, 2009) have reported highly elevated (and often correlated)
738 concentrations of Zn, Cd, Ga, Ag, and Pb associated with vent fluids of lower temperature and
739 pH than high-temperature black smoker vent fluids from the same vent field. The higher
740 concentrations of these metals have been attributed to remobilization of previously deposited
741 sulfide minerals within the subsurface (Fouquet et al., 1993; Tivey et al., 1995; Metz and Trefry,
742 2000; Craddock, 2009). Elevated concentrations of Zn, Cd and Ag concentrations among some
743 Tu'i Malila vent fluids (e.g., TM16, TM17) suggest sub-surface remobilization of Zn-bearing
744 massive sulfides within the Tu'i Malila vent field.

745 Analyses of Ga and In in hydrothermal vent fluids are rare. Among the data presented
746 here, concentrations of Ga in vent fluids from the mafic-hosted Tahi Moana-1 vent field (Ga =

747 2–15 nmol/kg) are lower than those from the basalt-andesite hosted ABE (Ga = 6–110 nmol/kg)
748 and Tu'i Malila vent fields (Ga = 6–130 nmol/kg) despite overlapping vent fluid temperatures
749 and pH (Fig. 7 Fig. S4, Table 8). This suggests that vent fluid Ga concentrations may be partially
750 controlled by host-rock lithology in addition to temperature and pH. However, the Ga
751 concentrations of ELSC and VFR vent fluids are broadly similar to vent fluid Ga concentrations
752 of 25 – 67 nmol/kg reported for vent fluids from the north and south Cleft segments of the
753 southern Juan de Fuca Ridge and the black smoker complex of the TAG hydrothermal mound
754 (Metz and Trefry, 2000). Vent fluid In concentrations reported here for ELSC and VFR vent
755 fluids (In = 30–240 nmol/kg; Table 8) are substantially higher than the 2.8 – 3.5 nmol/kg
756 reported for vent fluids from the Rainbow vent field, one of the few vent fields for which vent
757 fluid In concentrations have been analyzed (Douville et al., 2002). This comparison is surprising
758 given the higher temperatures (362–364°C), generally lower pH (pH (at 25°C) = 2.8–3.2), and
759 higher Cl concentrations (745–756 mmol/kg) of Rainbow vent fluids (Douville et al., 2002).
760

761 ## 6. CONCLUSIONS

762 Based on the comparison of Co, Ni, Ga, Ag, and In concentrations in black smoker
763 chimney linings and hydrothermal fluid chemistry presented in this paper, two factors stand out
764 as controlling trace element concentrations in chalcopyrite lining black smoker chimneys. The
765 first is the free ion activity ratio of trace elements relative to that of the major element being
766 replaced in the crystal lattice (e.g., Ag(I) for Cu(I), Ga(III) and In(III) for Fe(III)). In the case of
767 Ag replacing Cu, the free ion activity ratio of $\{Ag^+\}:\{Cu^+\}$ primarily reflects the total Ag:Cu
768 concentration ratio, which in turn reflects the combined effects of fluid pH and, in some cases,
769 elevated Ag concentrations that likely reflect remobilization of previously deposited sulfides. In

770 the case of Ga or In replacing Fe, the dominant control on the free ion activity ratios of
771 $\{Ga^{3+}\}:\{Fe^{3+}\}$ and $\{In^{3+}\}:\{Fe^{3+}\}$ is not the total concentrations of Ga or In, but rather the relative
772 concentrations of complexing ligands, Cl^- and OH^-. Among seafloor hydrothermal fluids
773 associated with black smoker chimneys, the variation in Cl^- concentrations is less than the
774 variation in OH^- concentrations associated with pH. Thus, the Ga and In contents of chalcopyrite
775 lining black smoker chimneys provides an effective proxy of vent fluid pH.

776 The second important controlling factor is crystallography, which is most evident in the
777 preferential partitioning of Co(II) and Ni(II) into Fe-rich Cu-Fe-S solid solutions. The influence
778 of crystallography on the partitioning of Co and Ni is demonstrated by correlations between the
779 Co and Ni concentrations and Cu:Fe ratios of black smoker chimney linings, as well as the
780 comparative lack of correlation between the Co and Ni concentrations of black smoker chimney
781 linings and hydrothermal fluid chemistry. Because of the strong effect of crystallography on Co
782 and Ni concentrations, these elements are unlikely to provide useful proxies of fluid chemistry
783 unless the effects of crystallography can more quantitatively understood and accounted for.

784 Overall, this study demonstrates the potential of using paired samples of black smoker
785 chimneys and hydrothermal vent fluids to investigate the partitioning of trace elements between
786 hydrothermal fluids and sulfide minerals and to develop proxies of important hydrothermal fluid
787 parameters such as pH. Additionally, this study demonstrates the utility of SIMS in achieving
788 quantitative measurements of trace elements in sulfide minerals (specifically chalcopyrite) at
789 high spatial resolutions and low detection limits. As such, SIMS has potential for use in a variety
790 of contexts where the trace element content of fine-grained sulfide minerals is unknown.
791 Avenues for future work include examination of additional trace elements and/or minerals,

investigation of SMS deposits beyond the linings of black smoker chimneys, and further analysis of the fundamental controls of trace element partitioning in sulfide minerals.

ACKNOWLEDGEMENTS

We thank the captains and crews of the R/V Atlantis III, the R/V Melville, the R/V Roger Revelle, the R/V Thomas G. Thompson, and the team of the ROV Jason II for their expertise in recovering fluid and SMS deposit samples from active vent fields. Margaret Sulanowska's help with sample preparation is gratefully acknowledged. This work was supported by the National Science Foundation [grant numbers OCE-1038135 to GNE and MKT, OCE-1038124, OCE-0241796, OCE-1233037 to JSS and NSF Graduate Research Fellowship to GNE]. The Northeast National Ion Microprobe Facility gratefully acknowledges support from the National Science Foundation Instrumentation and Facilities Program, Division of Earth Sciences, and from the Woods Hole Oceanographic Institution.

REFERENCES

Akinfiev, N. N., and Zotov, A. V. (2001) Thermodynamic description of chloride, hydrosulfide, and hydroxo complexes of Ag(I), Cu(I), and Au(I) at Temperatures of 25–500°C and pressures of 1–2000 bar. *Geochem. Int.* **39(10)**, 990–1006.

Benézéth, P., Diakonov, I. I., Pokrovski, G. S., Dandurand, J. L., Schott, J., and Khodakovsky, I. L. (1997) Gallium speciation in aqueous solution. Experimental study and modelling: Part 2. Solubility of α-GaOOH in acidic solutions from 150 to 250 C and hydrolysis constants of gallium (III) to 300 C. *Geochim. Cosmochim. Acta*, **61(7)**, 1345–1357.

Berglund, M. and Wieser, M. E. (2011) Isotopic compositions of the elements 2009 (IUPAC Technical Report). *Pure and Applied Chemistry,* **83(2)**, 397–410, doi:10.1351/PAC-REP-10-06-02

Bézos, A., Escrig, S., Langmuir, C. H., Michael, P. J., and Asimow, P. D. (2009) Origins of chemical diversity of back-arc basin basalts: A segment-scale study of the Eastern Lau

Spreading Center. *J. Geophys. Res.: Solid Earth (1978–2012)*, **114***, B06212, doi:*10.1029/2008JB005924

Binns, R. A. and Scott, S. D. (1993). Actively forming polymetallic sulfide deposits associated with felsic volcanic rocks in the eastern Manus back-arc basin, Papua New Guinea. *Econ. Geol.*, **88(8)**, 2226–2236.

Butler, I. B. and Nesbitt, R. W. (1999) Trace element distributions in the chalcopyrite wall of a black smoker chimney: insights from laser ablation inductively coupled plasma mass spectrometry (LA–ICP–MS). *Earth and Planet. Sci. Lett.*, **167(3)**, 335–345.

Butterfield, D. A., and Massoth, G. J. (1994) Geochemistry of north Cleft segment vent fluids: Temporal changes in chlorinity and their possible relation to recent volcanism. *J. Geophys. Res.: Solid Earth*, **99(B3)**, 4951–4968.

Craddock, P. R. (2009) Geochemical tracers of processes affecting the formation of seafloor hydrothermal fluids and deposits in the Manus back-arc basin. Ph.D. Thesis, MIT/WHOI Joint Program in Oceanography.

Danyushevsky, L., Robinson, P., Gilbert, S., Norman, M., Large, R., McGoldrick, P., and Shelley, M. (2011). Routine quantitative multi-element analysis of sulphide minerals by laser ablation ICP-MS: Standard development and consideration of matrix effects. *Geochemistry: Exploration, Environment, Analysis*, **11(1)**, 51–60.

Ding, K. and Seyfried, W. E. (1992) Determination of Fe-Cl complexes in the low pressure supercritical region (NaCl fluid): Iron solubility constraints on pH of subseafloor hydrothermal fluids. *Geochim. Cosmochim. Acta*, **56(10)**, 3681–3692, doi: 10.1016/0016-7037(92)90161-B.

Ding, K., Seyfried, W. E., Zhong, Z., Tivey, M. K., Von Damm, K. L., Bradley, A. M. (2005) The in situ pH of hydrothermal fluids at mid-ocean ridges. *Earth Planet Sci. Lett.*, **237**, 167–174.

Douville, E., Charlou, J. L., Oelkers, E. H., Bienvenu, P., Jove Colon, C. F., Donval, J. P., Fouquet, Y., Prieus, D., Appriou, P. (2002) The rainbow vent fluids (36°14'N, MAR) : the influence of ultramafic rocks and phase separation on trace metal content in Mid-Atlantic Ridge hydrothermal fluids. *Chem. Geol.*, **184**, 37–48.

Einaudi, M. T., Hedenquist, J. W., and Inan, E. E. (2003) Sulfidation state of fluids in active and extinct hydrothermal systems: transitions from porphyry to epithermal environments. In

Special Publication-Society of Economic Geologists, **10** (eds. S.F. Simmons, I. Graham). Society of Economic Geologists, 285–314.

Elthon, D., Ross, D. K., and Meen, J. K. (1995). Compositional variations of basaltic glasses from the Mid-Cayman Rise Spreading Center. *J. Geophys. Res.: Solid Earth*, **100(B7)**, 12497–12512.

Escrig, S., Bézos, A., *Goldstein,* S. L., Langmuir, C. H., and Michael, P. J. *(*2009*)* Mantle source variations beneath the Eastern Lau Spreading Center and the nature of subduction components in the Lau basin–Tonga arc system, *Geochem. Geophys. Geosyst.,* **10**, *Q04014, doi:*10.1029/2008GC002281.

Evans, G. N., Tivey, M. K., Seewald, J. S., and Wheat, C. G. (2017). Influences of the Tonga Subduction Zone on Seafloor Massive Sulfide Deposits along the Eastern Lau Spreading Center and Valu Fa Ridge. *Geochim. et Cosmochim. Acta*., **215,** 214–246.

Ferrini, V. L., *Tivey,* M. K., Carbotte, S. M., *Martinez,* F. , *and* Roman, C. *(*2008*)* Variable morphologic expression of volcanic, tectonic, and hydrothermal processes at six hydrothermal vent fields in the Lau back-arc basin, *Geochem. Geophys. Geosyst., **9**, Q07022, doi:*10.1029/2008GC002047.

Fouquet, Y., von Stackelberg, U., Charlou, J. L., Erzinger, J., Herzig, P. M., Mühe, R., and Wiedicke, M. (1993) Metallogenesis in back-arc environments: the Lau Basin example. *Econ. Geol.*, **88(8)**, 2154–2181.

Frenzel, G., Muhe, R., and Stoffers, P. (1990). Petrology of the volcanic rocks from the Lau Basin, southwest Pacific. *Geol. Jahrb*, **92**, 395–479.

Goh, S. W., Buckley, A. N., Skinner, W. M., Fan, L-J. (2006) An X-ray photoelectron and absorption spectroscopic investigation of the electron structure of cubanite, $CuFe_2S_3$, *Phys. Chem. Minerals*, **37(6)**, 389–405.

Goldfarb, M. S., Converse, D. R. Holland, H. D. and Edmond, J. M. (1983) The genesis of hot spring deposits on the East Pacific Rise, 21° N, *Econ. Geol. Monogr.*, **5**, 184–197.

Greenwood, N. N., and Whitfield, H. J. (1968) Mössbauer effect studies on cubanite ($CuFe_2S_3$) and related iron sulphides, *J. Chem. Soc.: Inorganic, Phys., Theoret.,* **0**, 1697-1699. doi: 10.1039/J19680001697.

Hannington, M. D., Jonasson, I. R., Herzig, P. M., and Petersen, S. (1995) Physical and chemical processes of seafloor mineralization at mid-ocean ridges. In *Seafloor hydrothermal systems: physical, chemical, biological, and geological interactions* (eds. S. E. Humphris, R. A. Zierenberg, L. S. Mullineaux, and R. E. Thomson), American Geophysical Union, Washington, D. C.. pp. 115–157. doi: 10.1029/GM091p0115.

907
908 Haymon, R. M. (1983) Growth history of hydrothermal black smoker chimneys. Nature, **301**,
909 695–698.
910
911 Huston, D. L., Sie, S. H., Suter, G. F., Cooke, D. R., and Both, R. A. (1995). Trace elements in
912 sulfide minerals from eastern Australian volcanic-hosted massive sulfide deposits; Part I,
913 Proton microprobe analyses of pyrite, chalcopyrite, and sphalerite, and Part II, Selenium
914 levels in pyrite; comparison with delta 34 S values and implications for the source of
915 sulfur in volcanogenic hydrothermal systems. *Econ. Geol.*, **90(5)**, 1167–1196.
916
917 Jenner, G. A., Cawood, P. A., Rautenschlein, M., and White, W. M. (1987). Composition of
918 back-arc basin volcanics, Valu Fa Ridge, Lau Basin: evidence for a slab-derived
919 component in their mantle source. *J. Volcanology Geothermal Res.*, **32(1-3)**, 209–222.
920
921 John, S.G., Rouxel, O.J., Craddock, P.R., Engwall, A.M., Boyle, E.A. (2008). Zinc stable
922 isotopes in seafloor hydrothermal vent fluids and chinmeys. *Earth. Planet. Sci. Lett.*,
923 **269(1-2)**, 17–28.
924
925 Johnson, H. P., Hutnak, M., Dziak, R. P., Fox, C. G., Urcuyo, I., Cowen, J. P., Nabelek, J., and
926 Fisher, C. (2000). Earthquake-induced changes in a hydrothermal system on the Juan de
927 Fuca mid-ocean ridge. *Nature*, **407(6801)**, 174–177.
928
929 Johnson, J. W., Oelkers, E. H., and Helgeson, H. C. (1992) SUPCRT92: A software package for
930 calculating the standard molal thermodynamic properties of minerals, gases, aqueous
931 species, and reactions from 1 to 5000 bar and 0 to 1000 C. *Computers Geosci.,* **18(7)**,
932 899–947.
933
934 Kamenetsky, V. S., Binns, R. A., Gemmell, J. B., Crawford, A. J., Mernagh, T. P., Maas, R., and
935 Steele, D. (2001). Parental basaltic melts and fluids in eastern Manus backarc basin:
936 Implications for hydrothermal mineralisation. *Earth Planet. Sci. Lett.*, **184(3)**, 685–702.
937
938 Karsten, J. L., Delaney, J. R., Rhodes, J. M., and Liias, R. A. (1990). Spatial and temporal
939 evolution of magmatic systems beneath the Endeavour Segment, Juan de Fuca Ridge:
940 Tectonic and petrologic constraints. *J. Geophys. Res.: Solid Earth*, **95(B12)**, 19235–
941 19256.
942
943 Kawasumi, S. and Chiba, H. (2017) Redox state of seafloor hydrothermal fluids and its effect on
944 sulfide mineralization. *Chem. Geol.*, **451**, 25–37.
945
946 Keith, M. Haase, K. M., Schwarz-Schampera, U., Klemd, R., Petersen, S., and Bach, W. (2014)
947 Effects of temperature, sulfur, and oxygen fugacity on the composition of sphalerite from
948 submarine hydrothermal vents, *Geology*, **42(8)**, 699–702, doi: 10.1130/G35655.1
949
950 Keith, M. Hächel, F., Haase, K. H., Schwarz-Schampera, U., Klemd, R. (2016) Trace element
951 systematics of pyrite from submarine hydrothermal vents, *Ore Geol. Rev.*, **72**, 728–745.

Kristall, B., Nielsen, D., Hannington, M. D., Kelley, D. S., Delaney, J. R. (2011) Chemical microenvironments within sulfide structures from the Mothra Hydrothermal Field: Evidence from high-resolution zoning of trace elements, *Chem. Geol.*, **290(1–2)**, 12–30.

Kojima, S. and Sugaki, A. (1985) Phase Relations in the Cu-Fe-Zn-S System between 500° and 300°C under Hydrothermal Conditions. *Econ. Geol.*, **80**, 158–171.

Krasnov, S., Poroshina, I., Cherkashev, G., Mikhalsky, E., and Maslov, M. (1997). Morphotectonics, volcanism and hydrothermal activity on the East Pacific Rise between 21 12′ S and 22 40′ S. *Marine Geophys. Res.*, **19(4)**, 287–317.

Langmuir, C., Humphris, S., Fornari, D., Van Dover, C., Von Damm, K. L., Tivey, M. K., Colodner, D., Charlou, J. –L. Desonie, D., Wilson, C., and Fouquet, Y. (1997). Hydrothermal vents near a mantle hot spot: the Lucky Strike vent field at 37 N on the Mid-Atlantic Ridge. *Earth Planetary Sci. Lett.*, **148(1-2)**, 69–91.

Langmuir, C. H., Bézos, A., Escrig, S., and Parman, S. W. (2006) Chemical systematics and hydrous melting of the mantle in back-arc basins. In *Back-Arc Spreading Systems: Geological, Biological, Chemical, and Physical Interactions* (eds. D. M. Christie, C. R. Fisher, S.-M. Lee, and S. Givens) Geophysical Monograph Series, vol. 166, American Geophysical Union, Washington, DC. pp. 87–146.

Layne, G., Tivey, M. K., and Humphris, S. E. (2005) Trace metal concentrations in common sulfide minerals using SIMS. *Fifteenth Annual V. M. Goldschmidt Conference* Abstracts, A55.

Lilley, M. D., Butterfield, D. A., Lupton, J. E. and Olson, E. J., (2003) Magmatic events can produce rapid changes in hydrothermal vent chemistry. *Nature*. **422**, 878–881.

Lusk, J. and Bray, D. M. (2002) Phase relations and the electrochemical determination of sulfur fugacity for selected reactions in the Cu-Fe-S and Fe-S systems at 1 bar and temperatures between 185 and 460 °C. *Chem. Geol.* **192**. 227–248.

Martinez, F. and Taylor, B. (2002) Mantle wedge control on back-arc crustal accretion. *Nature*. **416**, 417-420.

Maslennikov, V. V., Maslennikova, S. P., Large, R. R., and Danyushevsky, L. V. (2009) Study of trace element zonation in vent chimneys from the Silurian Yaman-Kasy volcanic-hosted massive sulfide deposit (Southern Urals, Russia) using laser ablation-inductively coupled plasma mass spectrometry (LA-ICPMS). *Econ. Geol.*, **104(8)**, 1111–1141.

McDermott, J. M., Ono, S., Tivey, M. K., Seewald, J. S., Shanks III, W. C., Solow, A. R. (2015) Identification of sulfur sources and isotopic equilibria in submarine hot-springs using multiple sulfur isotopes. *Geochim. Cosmochim, Acta*, **160(2015)**, 169–187.

McDermott, J. M., Sylva, S. P., Ono, S., German, C. R., Seewald, J. S., (2018) Geochemistry of fluids from Earth's deepest ridge-crest hot-springs: Piccard hydrothermal field, Mid-Cayman Rise. *Geochim. Cosmochim. Acta*, **228(1)**, 95–118.

McIntire, W. L. (1963) Trace element partition coefficients—a review of theory and applications to geology. *Geochim. Cosmochim. Acta*, **27**, 1209–1264.

Metz, S. and Trefry, J. H. (2000). Chemical and mineralogical influences on concentrations of trace metals in hydrothermal fluids. *Geochim. Cosmochim. Acta*, **64(13)**, 2267–2279.

Mottl, M. J., Seewald, J. S., Wheat, C. G., Tivey, M. K., Michael, P. J., Proskurowski, G., McCollom, M., Reeves, E., Sharkey, S., You, C.-F., Chan, L.-H., and Pichler, T. (2011) Chemistry of hot springs along the Eastern Lau Spreading Center. *Geochim Cosmochim. Acta*, **75(4)**, 1013–1038.

O'Grady, K. M. (2001) The Geochemical Controls on Hydrothermal Vent Fluid Chemistry from Two Areas on the Ultrafast-Spreading Southern East Pacific Rise, Master's thesis, University of New Hampshire.

Ono, S., Shanks, W.C., Rouxel, O.J., Rumble, D. (2007) S-33 constraints on the seawater sulfate contribution in modern seafloor hydrothermal vent sulfides. *Geochim. Cosmochim. Acta*, **71(5)**, 1170–1182.

Pearce, C. I., Pattrick, R. A. D., Vaughan, D. J., Henderson, C. M. B., van der Laan, G. (2006) Copper oxidation state in chalcopyrite: Mixed Cu d^9 and d^{10} characteristics. *Geochim. Cosmochim. Acta*, **70(18)**, 4634–4642.

Pokrovski, G. S., Roux, J., Ferlat, G., Jonchiere, R., Seitsonen, A. P., Vuilleumier, R., Hazemann, J-L. (2013) Silver in geological fluids from in situ X-ray absorption spectroscopy and first-principles molecular dynamics. *Geochim. Cosmochim. Acta*, **106**, 501–523.

Reeves, E. P., Seewald, J. S., Saccocia, P., Bach, W., Craddock, P. R., Shanks, W. C., Sylva. S., Walsh, E., Pichler, T., and Rosner, M. (2011) Geochemistry of hydrothermal fluids from the PACMANUS, Northeast Pual and Vienna Woods hydrothermal fields, Manus Basin, Papua New Guinea. *Geochim. Cosmochim. Acta*, **75(4)**, 1088–1123.

Rouxel, O. J., Fouquet, Y., Ludden, J. H. (2004) Copper Isotope Systematics of the Lucky Strike, Rainbow, and Logatchev Sea-Floor Hydrothermal Fields on the Mid-Atlantic Ridge, *Econ. Geol.*, **99(3)**, 585–600. doi: 10.2113/gsecongeo.99.3.585.

Rouxel, O., Shanks III, W.C., Bach, W., Edwards, K.J. (2008). Integrated Fe- and S-isotope study of seafloor hydrothermal vents at East Pacific Rise 9-10°N. *Chem. Geol.*, **252(3-4)**:

214–227.

Ryan, C. G. (2001). Developments in dynamic analysis for quantitative PIXE true elemental imaging. *Nuclear Instruments and Methods in Physics Research Section B: Beam Interactions with Materials and Atoms*, **181(1)**, 170–179.

Sack, R. O., and Ebel, D. S. (2006) Thermochemistry of sulfide mineral solutions. In *Reviews in mineralogy and geochemistry*, **61(1)** (ed. D.J. Vaughan). Geochemical Society and Mineralogical Society of America. pp. 265–364.

Schmidt, K., Koschinsky, A., Garbe-Schönberg, D., M. de Caravalho, L., Seifert, R. (2007) Geochemistry of hydrothermal fluids from the ultramafic-hosted Logatchev hydrothermal field, (15°N on the Mid-Atlantic Ridge): Temporal and spatial investigation. *Chem. Geol.*, **242**, 1–21.

Schmidt, K., Garbe-Schönberg, D., Koschinsky, A., Strauss, H., Jost, C. L., Klevenz, V., Königer, P. (2011) Fluid elemental and stable isotope composition of the Niebelungen hydrothermal field, (8°18'S, Mid-Atlantic Ridge): Constraints on fluid-rock interaction in heterogeneous lithosphere. *Chem. Geol.*, **230(1-2)**, 1–18.

Seewald, J. S. (2017) Chemical composition of hydrothermal fluids collected on RV/Roger Revelle RR1507 in the Eastern Lau Spreading Center and Valu Fa Ridge, April-May 2015 (Functional microbial dynamics of vent deposits project) Biological and Chemical Oceanography Data Management Office (BCO-DMO) Dataset version 2017-01-13 http://lod.bco-dmo.org/id/dataset/674750 (accessed, May 2017).

Seewald, J. S., and Seyfried, W. E. (1990). The effect of temperature on metal mobility in subseafloor hydrothermal systems: constraints from basalt alteration experiments. *Earth Planetary Sci. Lett.*, **101(2–4)**, 388–403.

Seewald, J. S., Doherty, K. W., Hammar, T. R., and Liberatore, S. P. (2002) A new gas-tight isobaric sampler for hydrothermal fluids. *Deep Sea Research Part I: Oceanographic Research Papers*, **49(1),** pp. 189–196.

Seewald, J. S., Cruse, A., Saccocia, P. (2003) Aqueous volatiles in hydrothermal fluids from the Main Endeavour Field, northern Juan de Fuca Ridge: temporal variability following earthquake activity. *Earth Planteary Lett.*, **216(4)**, 575–590. doi: 10.1016/S0012-821X(03)00543-0.

Seyfried, W. E. and Ding, K. (1993) The effect of redox on the relative solubilities of copper and iron in Cl-bearing aqueous fluids at elevated temperatures and pressures: An experimental study with application to subseafloor hydrothermal systems. *Geochim. Cosmochim. Acta*, **57(9)**, 1905–1917.

Seyfried, W. E., Seewald, J. S., Berndt, M. E., Ding, K., and Foustoukos, D. I. (2003). Chemistry of hydrothermal vent fluids from the Main Endeavour Field, northern Juan de Fuca Ridge:

Geochemical controls in the aftermath of June 1999 seismic events. *J. Geophys. Res.: Solid Earth*, **108**(B9).

Shock, E. L., Sassani, D. C., Willis, M., and Sverjensky, D. A. (1997). Inorganic species in geologic fluids: correlations among standard molal thermodynamic properties of aqueous ions and hydroxide complexes. *Geochim. Cosmochim. Acta*, **61(5)**, 907–950.

Sinton, J. M., Ford, L. L., Chappell, B., and McCullouch, M. T. (2003). Magma genesis and mantle heterogeneity in the Manus back-arc basin, Papua New Guinea. *J. Petrology*, **44(1)**, 159–195.

Sverjensky, D. A., Shock, E. L., and Helgeson, H. C. (1997). Prediction of the thermodynamic properties of aqueous metal complexes to 1000 C and 5 kb. *Geochim. Cosmochim. Acta*, **61(7)**, 1359–1412.

Takai, K., Nunoura, T., Ishibashi, J.-I., Lupton, J., Suzuki, R., Hamasaki, H., Ueno, Y., Kawagucci, S., Gamo, T., Suzuki, Y., Hirayama, H., and Horikoshi, K. (2008) Variability in the microbial communities and hydrothermal fluid chemistry at the newly discovered Mariner hydrothermal field, southern Lau Basin. J. *Geophys. Res.,* **113***, G02031, doi:*10.1029/2007JG000636.

Tivey, M. K. (1995) The influence of hydrothermal fluid composition and advection rates on black smoker chimney mineralogy: Insights from modeling transport and reaction. *Geochim. Cosmochim. Acta.*, **59(10)**, 1933–1949.

Tivey, M.K. (2004) Environmental conditions within active seafloor vent structures: sensitivity to vent fluid composition and fluid flow. In Wilcock, W., Cary, C., DeLong, E., Kelley, D., Baross, J. (Eds.) Subseafloor Biosphere at Mid-Ocean Ridges, Geophysical Monograph Series, No. 144. American Geophysical Union, Washington, DC, pp. 137–152.

Tivey, M. K., Humphris, S. E., Thompson, G., Hannington, M. D., and Rona, P. A. (1995). Deducing patterns of fluid flow and mixing within the TAG active hydrothermal mound using mineralogical and geochemical data. *J. Geophys. Res.*, **100(B7)**, 12527–12555.

Tivey, M. K., Stakes, D. S., Cook, T. L., Hannington, M. D., and Petersen, S. (1999) A model for growth of steep-sided vent structures on the Endeavour Segment of the Juan de Fuca Ridge: Results of a petrologic and geochemical study. *J. Geophys. Res: Solid Earth (1978–2012)*, **104(B10),** 22859–22883.

Trefry, J. H., Butterfield, D. B., Metz, S., Massoth, G. J., Trocine, R. P., and Feely R. A. (1994) Trace metals in hydrothermal solutions from Cleft segment on the southern Juan de Fuca Ridge. *J. Geophys. Res.***99**, 4925–4935.

Tunaboylu, K., Schwarzenbach, G., 1970. Die Löslichkeit von Indiumsulfid. *Chimia* (Switzerland) **24**, 424–427.

Vallier, T. L., Jenner, G. A., Frey, F. A., Gill, J. B., Davis, A. S., Volpe, A. M., Hawkins, J. W., Morris, J.D., Cawood, P.A., Morton, J. L., Scholl, D.W., Rautenschlein, M.,White, Williams, W.M., Stevenson, A.J., White, L.D. (1991). Subalkaline andesite from Valu Fa Ridge, a back-arc spreading center in southern Lau Basin: petrogenesis, comparative chemistry, and tectonic implications. *Chem. Geol.*, **91(3)**, 227–256.

Von Damm, K. L., Edmond, J. M., Grant, B., Measures, C. I., Walden, B., and Weiss, R. F. (1985). Chemistry of submarine hydrothermal solutions at 21° N, East Pacific Rise. *Geochim. Cosmochim. Acta*, **49(11)**, 2197–2220.

Wohlgemuth-Ueberwasser, C. C., Viljoen, F., Petersen, S., and Vorster, C. (2015). Distribution and solubility limits of trace elements in hydrothermal black smoker sulfides: An in-situ LA-ICP-MS study. *Geochim. Cosmochim. Acta*, **159**, 16–41.

Wood, S. A. and Samson, I. M. (2006) The aqueous geochemistry of gallium, germanium, indium, and scandium. *Ore Geol. Rev.*, **28(1)**, 57–102.

Wolery, T. J. (1992) EQ3/6: A software package for geochemical modeling of aqueous systems: package overview and installation guide (version 7.0). Livermore, CA: Lawrence Livermore National Laboratory.

Figure 1. (A) Schematic representation of a black smoker chimney showing massive sulfide chimney lining in contact with hydrothermal vent fluids (J. Doucette, WHOI Graphic Services, after Haymon, 1983). (B) Photomicrograph of sample J2-216-16-R1 (Fenway, F3) showing scale of SIMS spots. Photomicrograph was taken following SIMS measurements and removal of gold coating. The fluid conduit adjascent to the chimney lining has been filled with epoxy.

Figure 2. Mass vs. secondary ion intensity for the relevant mass intervals containing $^{59}Co^{+}$, $^{60}Ni^{+}$, $^{69}Ga^{+}$, $^{63}Cu^{16}O^{+}$, $^{109}Ag^{+}$, and $^{115}In^{+}$. Peaks appear as measured in chalcopyrite from the innermost lining of black smoker chimney sample Alv3299-6-1 from the 17°34'S vent field on the southern East Pacific Rise. Mass resolving power is ~10,000. Actual masses of target ions and those of potential interferences are labeled as calculated from tables in Berglund and Wieser (2011).

Figure 3. SIMS calibration curves obtained by plotting trace element concentrations of picked chalcopyrite grains measured by inductively coupled plasma mass spectrometry (ICP-MS) vs. secondary ion ratios measured by secondary ion mass spectrometry (SIMS)of the same samples. Samples used in forming SIMS calibration curves marked in black. Additional measured samples not used in forming SIMS calibration curves marked in white. Also shown are linear regression lines used in calculations (solid) and 95% confidence intervals (stippled).

Figure 4. SIMS measurements of Co and Ni on a log vs. log scale. Selected samples are labeled with molar Cu:Fe ratios obtained by electron microprobe analyses. Uncertainties in SIMS count ratios reflect standard errors (1σ) of multiple SIMS spots on the same sample. ELSC = Eastern Lau Spreading Center; VFR = Valu Fa Ridge; EMB = Eastern Manus Basin; EPR = East Pacific Rise; JdF = Juan de Fuca Ridge; MCR = Mid-Cayman Rise.

Figure 5. Cu:Fe molar ratio in black smoker chimney linings measured by electron microprobe (EMPA) vs. concentrations of Co and Ni in black in the same samples measured by SIMS. Also shown are regression lines calculated with (solid) and without (stippled) inclusion of MCR sample J2-613-16-R1. Right-hand plots are blowups of left-hand plots. EPR = East Pacific Rise; JdF = Juan de Fuca Ridge; MCR = Mid-Cayman Rise. Uncertainties in SIMS measurements reflect standard errors (1σ) of multiple SIMS spots on the same sample.

Figure 6. Vent fluid temperatures, pH, and metal concentrations of seafloor hydrothermal vent fluids obtained from scientific literature and results of this paper. Vent fluids that are samples with black smoker chimney linings analyzed by SIMS in this paper are identified with red dots.

References for: Lau Basin: Mottl et al. (2011); Seewald (2017); Evans et al., (2017); Manus Basin: Craddock (2009); Reeves et al. (2011); East Pacific Rise: Von Damm et al. (1985); Juan de Fuca Ridge: Trefry et al. (1994); Seyfried et al. (2003); Mid-Atlantic Ridge: Metz and Trefry (2000) ; Douville et al. (2002); Schmidt et al. (2007); Schmidt et al. (2011); Mid-Cayman Rise (MCR): McDermott et al. (2018).

Figure 7. Trace metal concentrations of seafloor hydrothermal vent fluids obtained from scientific literature and results of this paper. Vent fluids that are samples with black smoker chimney linings analyzed by SIMS in this paper are identified with red dots. References for: Lau Basin: Evans (2017); Manus Basin: Craddock (2009); East Pacific Rise: Von Damm et al. (1985); Juan de Fuca Ridge: Trefry et al. (1994); Seyfried et al. (2003); Mid-Atlantic Ridge: Metz and Trefry (2000); Douville et al. (2002); Schmidt et al. (2007); Schmidt et al. (2011); Mid-Cayman Rise (MCR): McDermott et al. (2018).

Figure 8. Ratios of free Ag^+:free Cu^+ in hydrothermal fluids calculated by EQ3/6 thermodynamic modeling vs. Ag concentrations in in paired black smoker chimney linings.. ELSC = Eastern Lau Spreading Center, VFR = Valu Fa Ridge; EMB = Eastern Manus Basin; JdF = Juan de Fuca Ridge; MCR = Mid-Cayman Rise. Also shown is the best-fit linear regression line (solid) and 95% confidence intervals (stippled).

Figure 9. Hydrothermal fluid pH at 25°C and at *in situ* temperatures (modeled using EQ3/6) vs. Ga, Ag, and In concentrations in in paired black smoker chimney linings. ELSC = Eastern Lau Spreading Center, VFR = Valu Fa Ridge; EMB = Eastern Manus Basin; JdF = Juan de Fuca Ridge; MCR = Mid-Cayman Rise. References for hydrothermal fluid pH are: Eastern Lau Spreading Center and Valu Fa Ridge (Seewald, 2017); Manus Basin: Craddock (2009), Reeves et al. (2011); Sully99 vent fluid from the Main Endeavour Field: Seyfried et al.(2003); BB5 vent fluid from the Beebe / Piccard vent field: McDermott et al. (2018).

1213 Uncertainties in SIMS count ratios reflect standard errors (1σ) of multiple SIMS spots on the same
1214 sample.
1215
1216 **Figure 10.** Thermodynamic stability diagrams from Wood and Samson (2006) showing pH vs. the log
1217 concentration of aqueous Ga complexes contributing to the solubility of GaOOH at 300°C at vapor
1218 saturated pressures using the thermodynamic data of Benézéth et al. (1997) and pH vs. the log
1219 concentration of aqueous In complexes contributing to the solubility of In_2S_3 at 20°C and 1M $NaClO_4$,
1220 total S = 0.01M using thermodynamic data from Tunaboylu and Schwarzenbach (1970). Red lines
1221 highlight the activities of free ions, Ga^{3+} and In^{3+}, as a function of pH.
1222
1223 **Figure 11.** Free ion activity ratios $\{Co^{2+}\}:\{Fe^{2+}\}$ and $\{Ni^{2+}\}:\{Fe^{2+}\}$ in hydrothermal fluids as calculated by
1224 EQ3/6 vs. Co and Ni concentrations in in paired black smoker chimney linings.. Also shown are total
1225 Co:Fe and Ni:Fe concentration ratios vs. Co and Ni concentrations in in paired black smoker chimney
1226 linings. X-axes cross at SIMS detection limits. ELSC = Eastern Lau Spreading Center, VFR = Valu Fa Ridge;
1227 EMB = Eastern Manus Basin; JdF = Juan de Fuca Ridge; MCR = Mid-Cayman Rise. Fluid data sources are:
1228 Eastern Lau Spreading Center (Seewald, 2017; this paper), Manus Basin (Craddock,2009), Main
1229 Endeavour Field (Seyfried et al.,2003), Mid-Cayman Rise (McDermott et al., 2018).
1230
1231 **Supplementary Figure S1.** Hydrothermal fluid pH (at 25°C) vs. Ag and Cu concentrations based on
1232 scientific literature and results of this paper. Fluids with chimney pairs analyzed in this paper are
1233 identified with red dots. ELSC = Eastern Lau Spreading Center, VFR = Valu Fa Ridge; EMB = Eastern
1234 Manus Basin; JdF = Juan de Fuca Ridge; MCR = Mid-Cayman Rise. References for: Lau Basin: Mottl et al.
1235 (2011); Seewald (2017); Evans et al. (2017); Manus Basin: Craddock (2009); Reeves et al. (2011); East
1236 Pacific Rise: Von Damm et al. (1985); Juan de Fuca Ridge: Trefry et al. (1994); Seyfried et al. (2003); Mid-

Atlantic Ridge: Metz and Trefry (2000); Douville et al. (2002); Schmidt et al. (2007); Schmidt et al. (2011); Mid-Cayman Rise (MCR): McDermott et al. (2018).

Supplementary Figure S2. Free ion activity ratios $\{Ga^{3+}\}:\{Fe^{3+}\}$ and $\{In^{3+}\}:\{Fe^{3+}\}$ in hydrothermal fluids from the Eastern Lau Spreading Center (ELSC) and Valu Fa Ridge (VFR) as calculated by EQ3/6 vs. Ga and In concentrations in in paired black smoker chimney linings. Also shown are total Ge:Fe and In:Fe concentration ratios vs. Ga and In concentrations in in paired black smoker chimney linings.

Supplementary Figure S3. Seafloor hydrothermal fluid temperatures, pH (at 25°C), and chlorinity vs. major and trace metal concentrations obtained from scientific literature and results of this paper. Fluids with chimney pairs analyzed in this paper by SIMS are indicated with red dots. BAB = Back-Arc Basins; EPR = East Pacific Rise; JdF = Juan de Fuca Ridge; MAR,B = basalt-hosted Mid-Atlantic Ridge (Snakepit, TAG, Logatchev); MAR,U = ultramafic-hosted Mid-Atlantic Ridge (Rainbow); MCR = Mid-Cayman Rise. References for: Lau Basin: Mottl et al. (2011); Seewald (2017); Evans et al. (2017); Manus Basin: Craddock (2009); Reeves et al. (2011); East Pacific Rise: Von Damm et al. (1985); Juan de Fuca Ridge: Trefry et al. (1994); Seyfried et al. (2003); Mid-Atlantic Ridge: Metz and Trefry (2000); Douville et al. (2002); Schmidt et al. (2007); Schmidt et al. (2011); Mid-Cayman Rise (MCR): McDermott et al. (2018).

Supplementary Figure S4. Seafloor hydrothermal fluid temperatures, pH (at 25°C), and chlorinity vs. trace metal concentrations obtained from scientific literature and results of this paper. Fluids with chimney pairs analyzed in this paper by SIMS are indicated with red dots. BAB = Back-Arc Basins; EPR = East Pacific Rise; JdF = Juan de Fuca Ridge; MAR,B = basalt-hosted Mid-Atlantic Ridge (Snakepit, TAG, Logatchev); MAR,U = ultramafic-hosted Mid-Atlantic Ridge (Rainbow); MCR = Mid-Cayman Rise. References for: Lau Basin: Mottl et al. (2011); Seewald (2017); Evans et al. (2017); Manus Basin: Craddock (2009); Reeves et al. (2011); East Pacific Rise: Von Damm et al. (1985); Juan de Fuca Ridge:

Trefry et al. (1994); Seyfried et al. (2003); Mid-Atlantic Ridge: Metz and Trefry (2000); Douville et al. (2002); Schmidt et al. (2007); Schmidt et al. (2011); Mid-Cayman Rise (MCR): McDermott et al. (2018).

Figure 1. (A) Schematic representation of a black smoker chimney showing massive sulfide chimney lining in contact with hydrothermal vent fluids (J. Doucette, WHOI Graphic Services, after Haymon, 1983). (B) Photomicrograph of sample J2-216-16-R1 (Fenway, F3) showing scale of SIMS spots. Photomicrograph was taken following SIMS measurements and removal of gold coating. The fluid conduit adjascent to the chimney lining has been filled with epoxy.

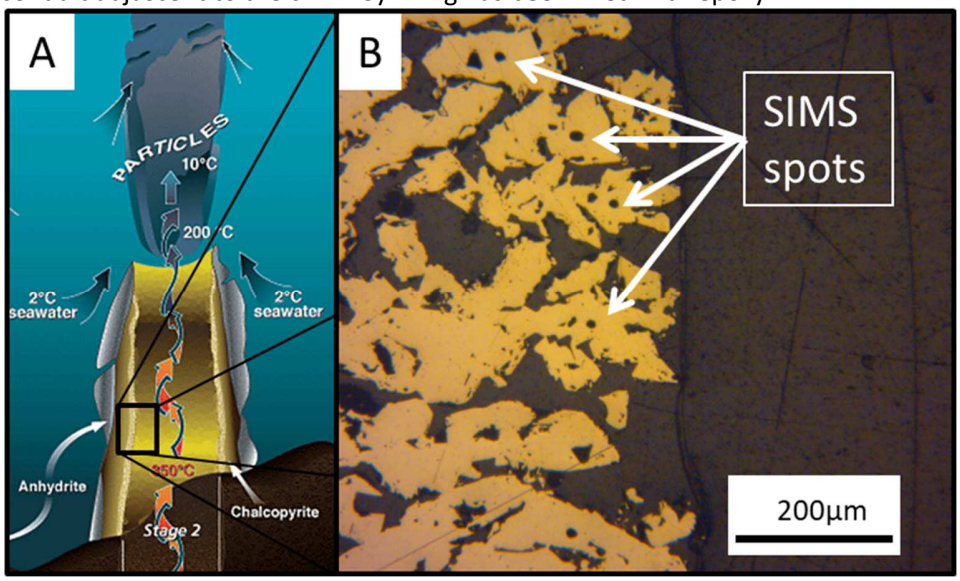

Figure 2. Mass vs. secondary ion intensity for the relevant mass intervals containing $^{59}Co^{+}$, $^{60}Ni^{+}$, $^{69}Ga^{+}$, $^{63}Cu^{16}O^{+}$, $^{109}Ag^{+}$, and $^{115}In^{+}$. Peaks appear as measured in chalcopyrite from the innermost lining of black smoker chimney sample Alv3299-6-1 from the 17°34'S vent field on the southern East Pacific Rise. Mass resolving power is ~10,000. Actual masses of target ions and those of potential interferences are labeled as calculated from tables in Berglund and Wieser (2011).

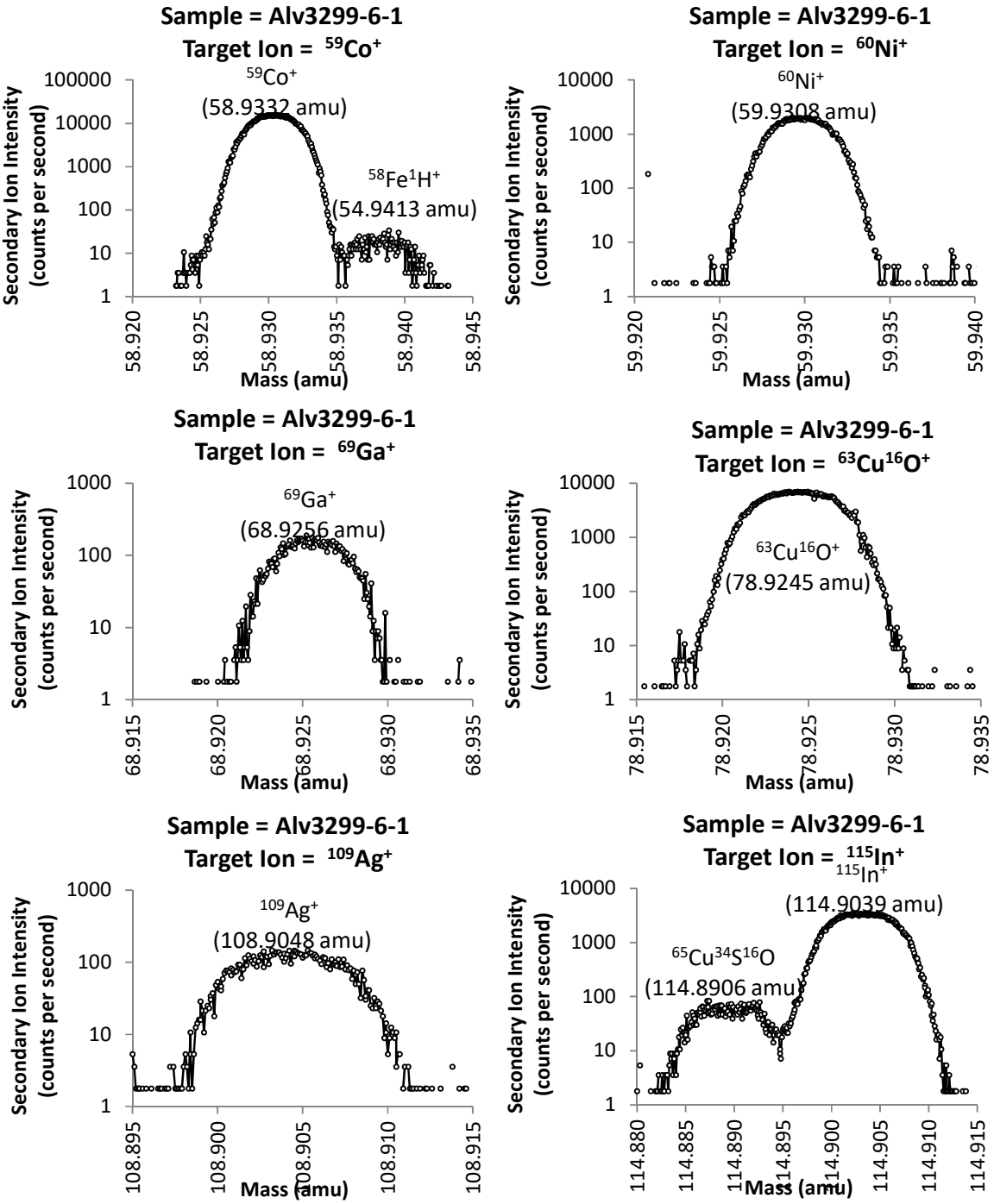

Figure 3. SIMS calibration curves obtained by plotting trace element concentrations of picked chalcopyrite grains measured by inductively coupled plasma mass spectrometry (ICP-MS) vs. secondary ion ratios measured by secondary ion mass spectrometry (SIMS)of the same samples. Samples used in forming SIMS calibration curves marked in black. Additional measured samples not used in forming SIMS calibration curves marked in white. Also shown are linear regression lines used in calculations (solid) and 95% confidence intervals (stippled).

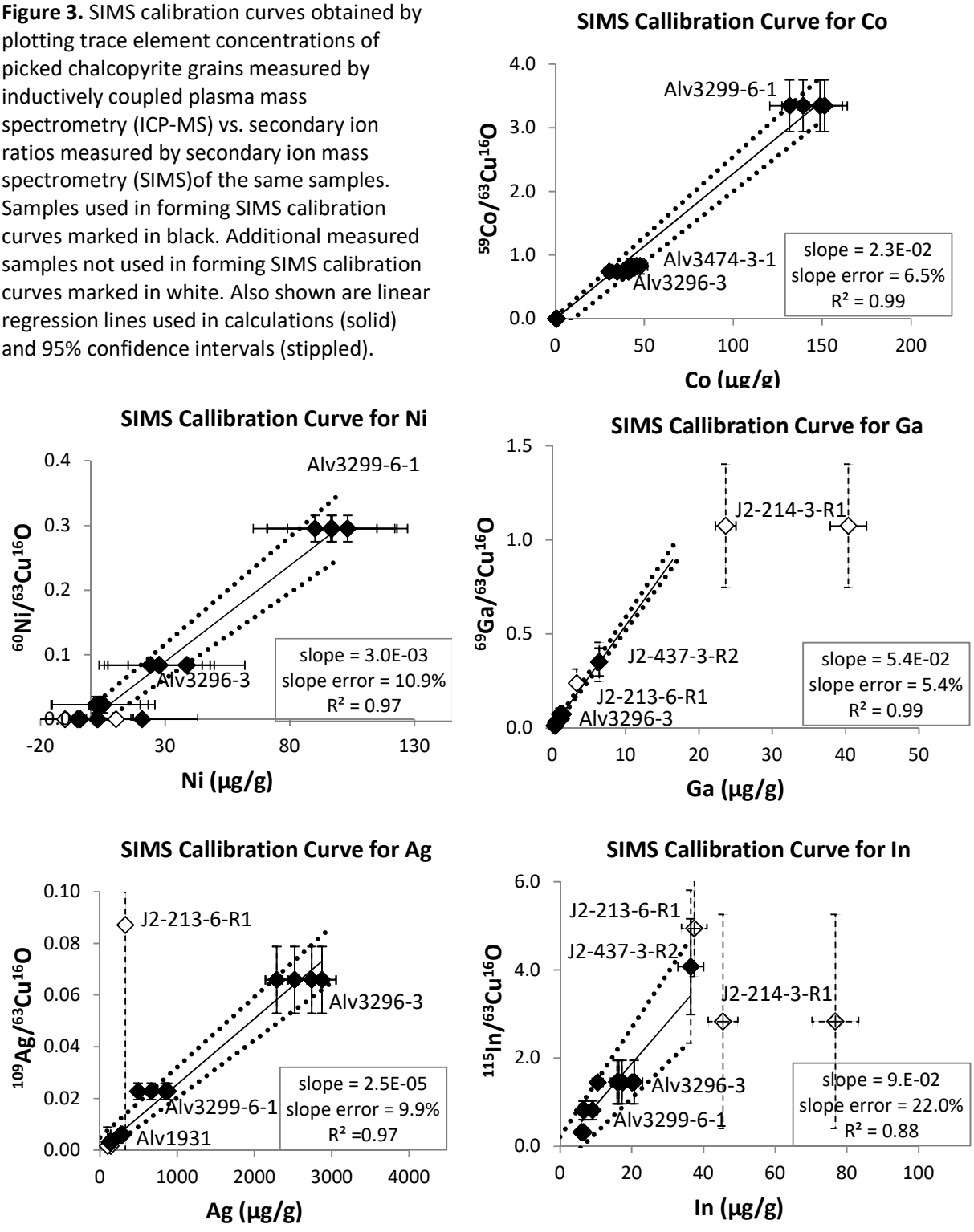

Figure 4. SIMS measurements of Co and Ni on a log vs. log scale. Selected samples are labeled with molar Cu:Fe ratios obtained by electron microprobe analyses. Uncertainties in SIMS count ratios reflect standard errors (1σ) of multiple SIMS spots on the same sample. ELSC = Eastern Lau Spreading Center; VFR = Valu Fa Ridge; EMB = Eastern Manus Basin; EPR = East Pacific Rise; JdF = Juan de Fuca Ridge; MCR = Mid-Cayman Rise.

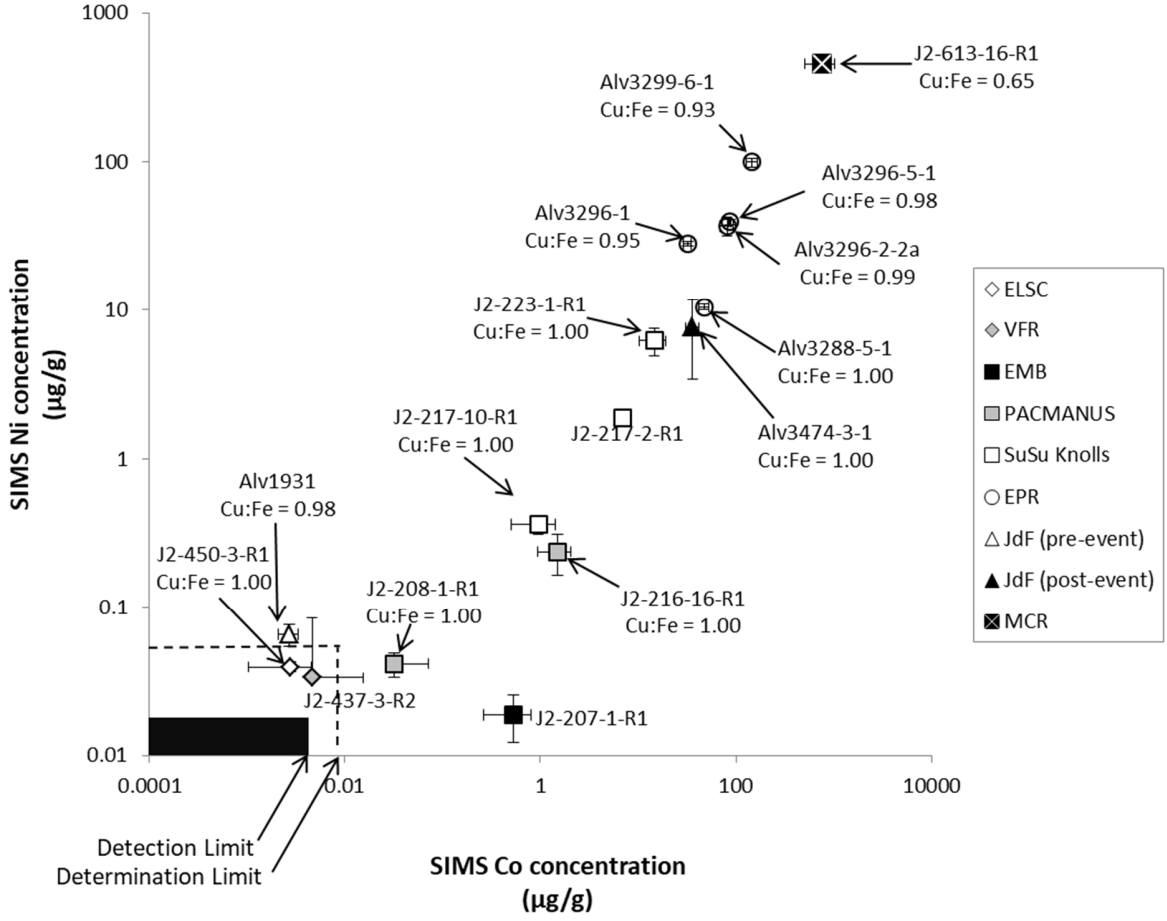

Figure 5. Cu:Fe molar ratio in black smoker chimney linings measured by electron microprobe (EMPA) vs. concentrations of Co and Ni in black in the same samples measured by SIMS. Also shown are regression lines calculated with (solid) and without (stippled) inclusion of MCR sample J2-613-16-R1. Right-hand plots are blowups of left-hand plots. EPR = East Pacific Rise; JdF = Juan de Fuca Ridge; MCR = Mid-Cayman Rise. Uncertainties in SIMS measurements reflect standard errors (1σ) of multiple SIMS spots on the same sample.

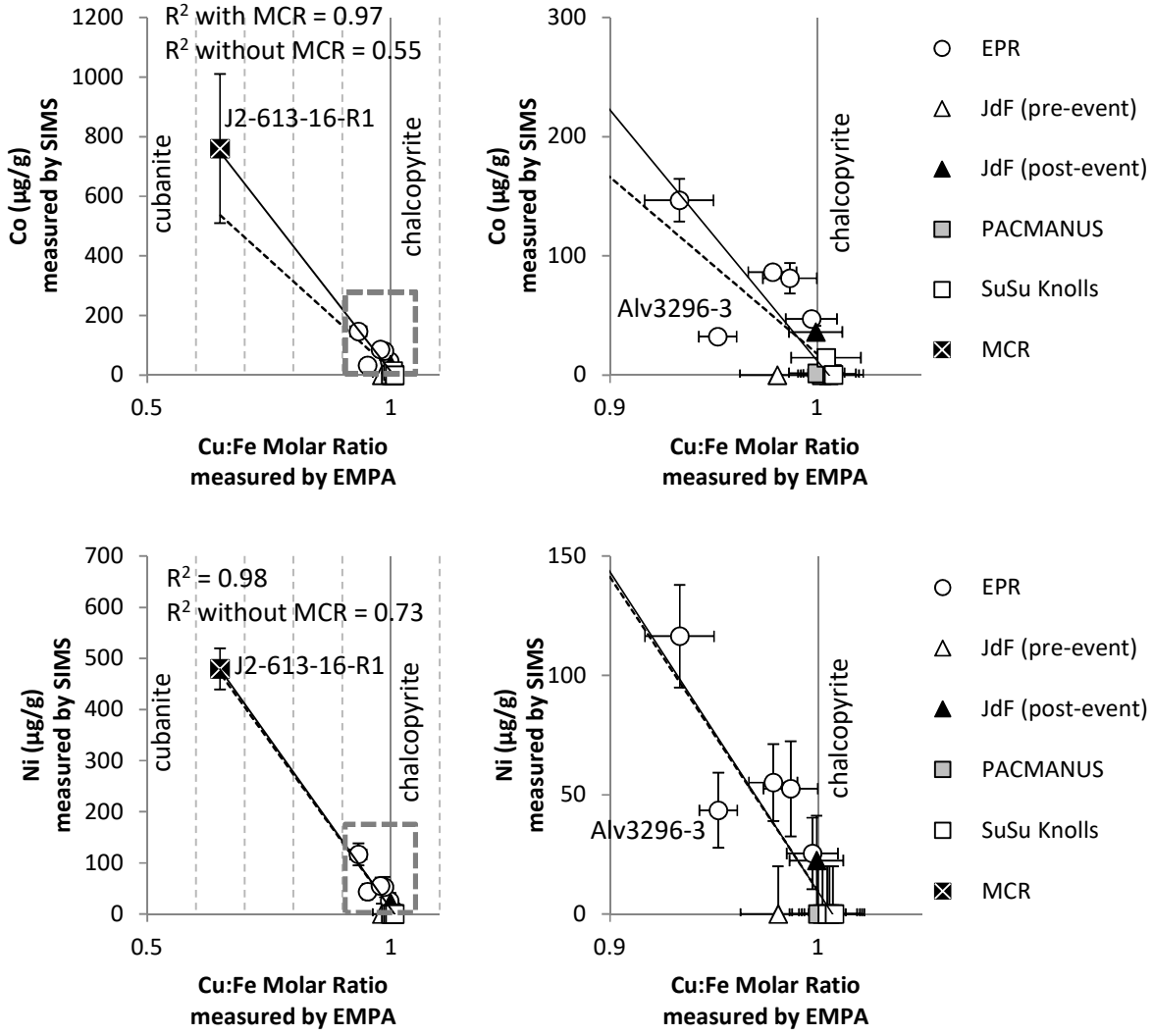

Figure 6. Vent fluid temperatures, pH, and metal concentrations of seafloor hydrothermal vent fluids obtained from scientific literature and results of this paper. Vent fluids that are samples with black smoker chimney linings analyzed by SIMS in this paper are identified with red dots.
References for: Lau Basin: Mottl et al. (2011); Seewald (2017); Evans et al., (2017); Manus Basin: Craddock (2009); Reeves et al. (2011); East Pacific Rise: Von Damm et al. (1985); Juan de Fuca Ridge: Trefry et al. (1994); Seyfried et al. (2003); Mid-Atlantic Ridge: Metz and Trefry (2000) ; Douville et al. (2002); Schmidt et al. (2007); Schmidt et al. (2011); Mid-Cayman Rise (MCR): McDermott et al. (2018).

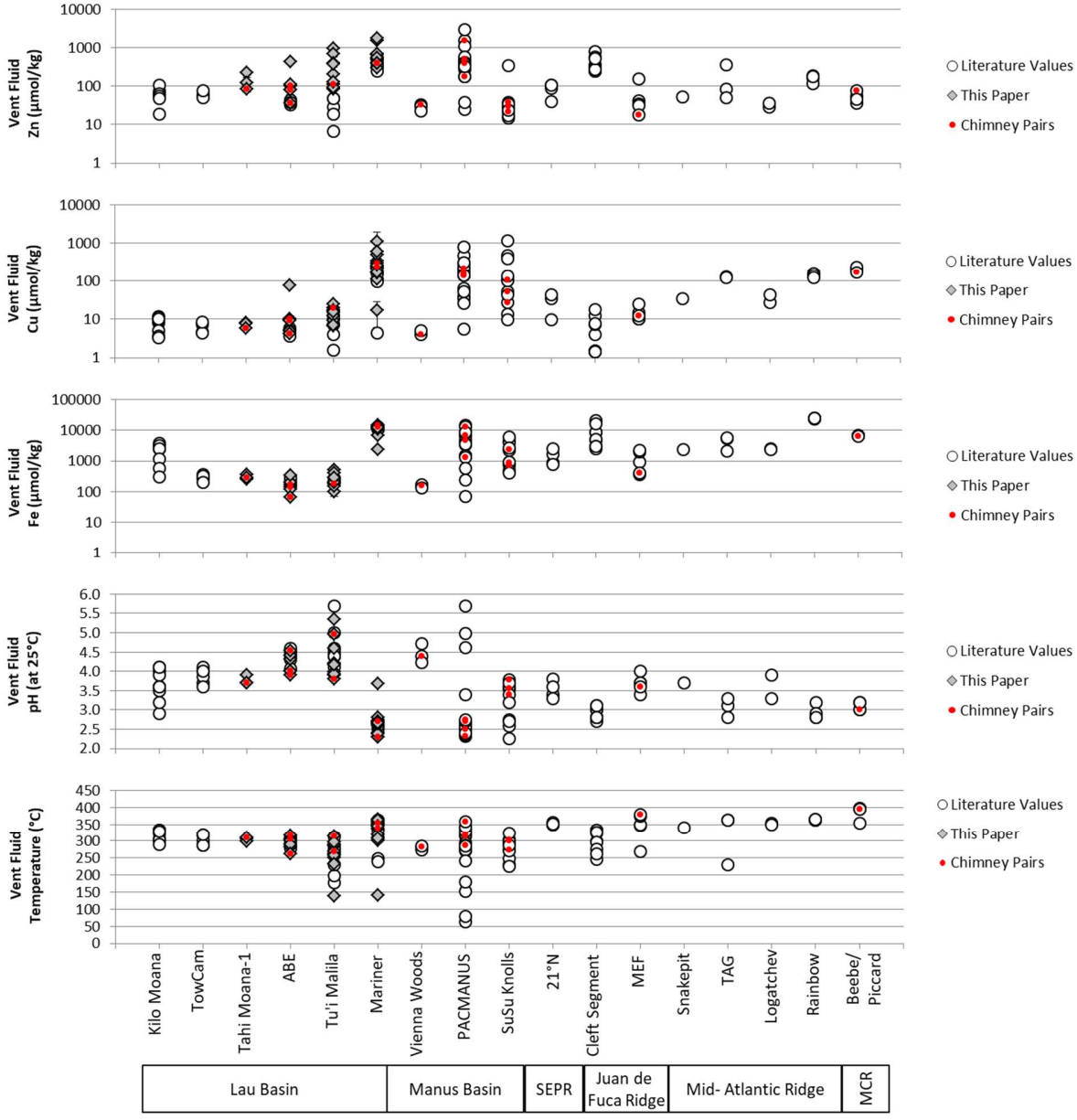

Figure 7. Trace metal concentrations of seafloor hydrothermal vent fluids obtained from scientific literature and results of this paper. Vent fluids that are samples with black smoker chimney linings analyzed by SIMS in this paper are identified with red dots. References for: Lau Basin: Evans (2017); Manus Basin: Craddock (2009); East Pacific Rise: Von Damm et al. (1985); Juan de Fuca Ridge: Trefry et al. (1994); Seyfried et al. (2003); Mid-Atlantic Ridge: Metz and Trefry (2000); Douville et al. (2002); Schmidt et al. (2007); Schmidt et al. (2011); Mid-Cayman Rise (MCR): McDermott et al. (2018).

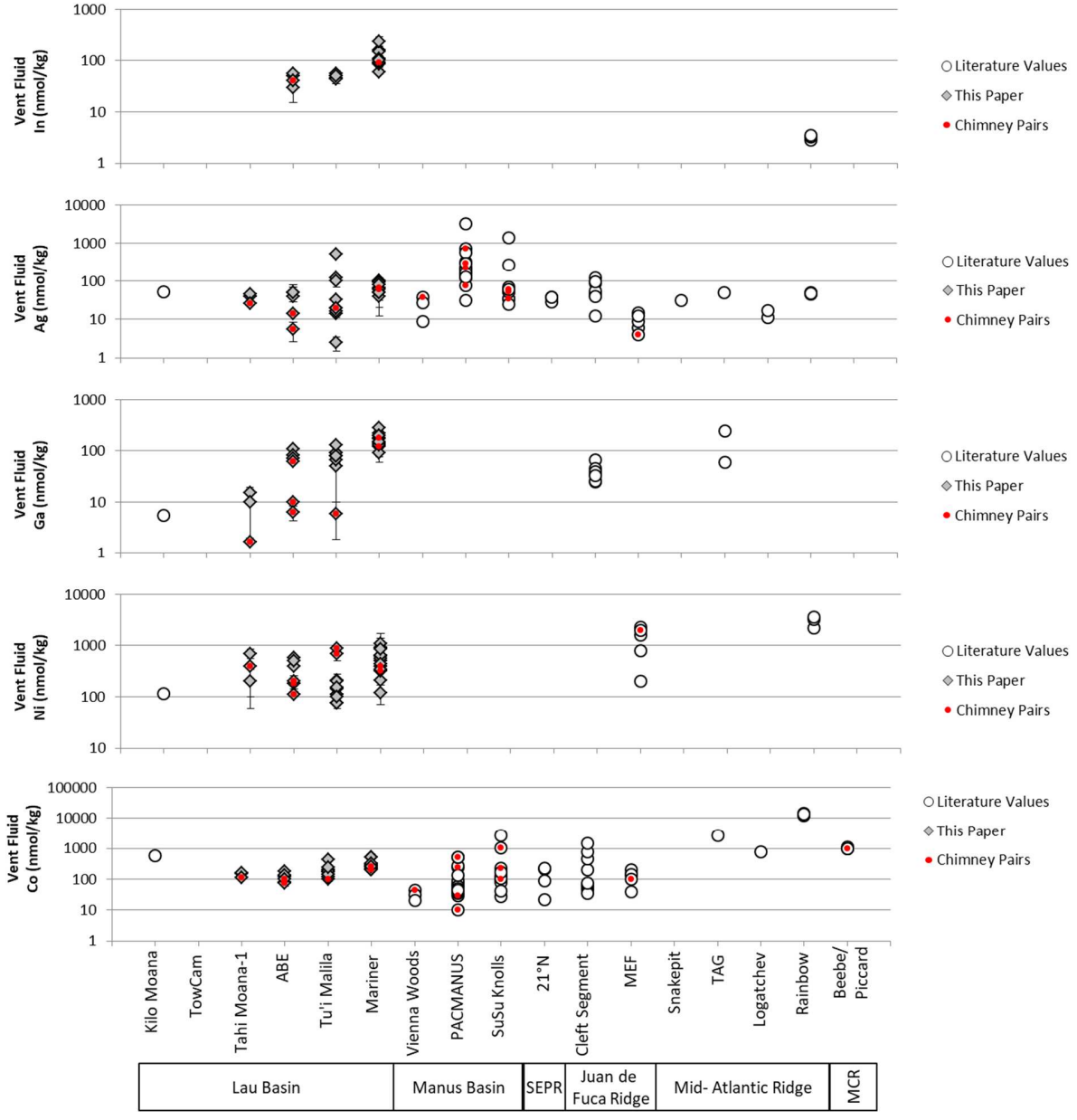

Figure 8. Ratios of free Ag^+:free Cu^+ in hydrothermal fluids calculated by EQ3/6 thermodynamic modeling vs. Ag concentrations in in paired black smoker chimney linings.. ELSC = Eastern Lau Spreading Center, VFR = Valu Fa Ridge; EMB = Eastern Manus Basin; JdF = Juan de Fuca Ridge; MCR = Mid-Cayman Rise. Also shown is the best-fit linear regression line (solid) and 95% confidence intervals (stippled).

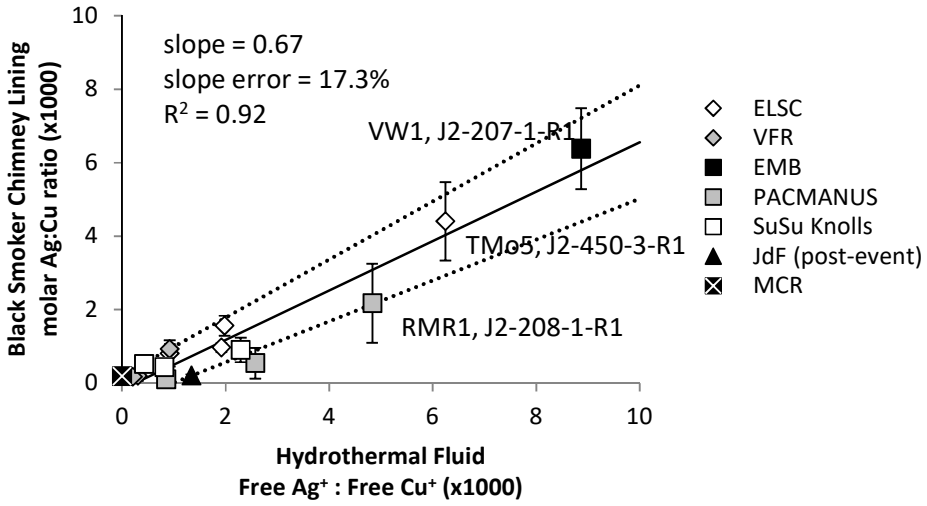

Figure 9. Hydrothermal fluid pH at 25°C and at *in situ* temperatures (modeled using EQ3/6) vs. Ga, Ag, and In concentrations in in paired black smoker chimney linings. ELSC = Eastern Lau Spreading Center, VFR = Valu Fa Ridge; EMB = Eastern Manus Basin; JdF = Juan de Fuca Ridge; MCR = Mid-Cayman Rise. References for hydrothermal fluid pH are: Eastern Lau Spreading Center and Valu Fa Ridge (Seewald, 2017); Manus Basin: Craddock (2009), Reeves et al. (2011); Sully99 vent fluid from the Main Endeavour Field: Seyfried et al.(2003); BB5 vent fluid from the Beebe / Piccard vent field: McDermott et al. (2018). Uncertainties in SIMS count ratios reflect standard errors (1σ) of multiple SIMS spots on the same sample.

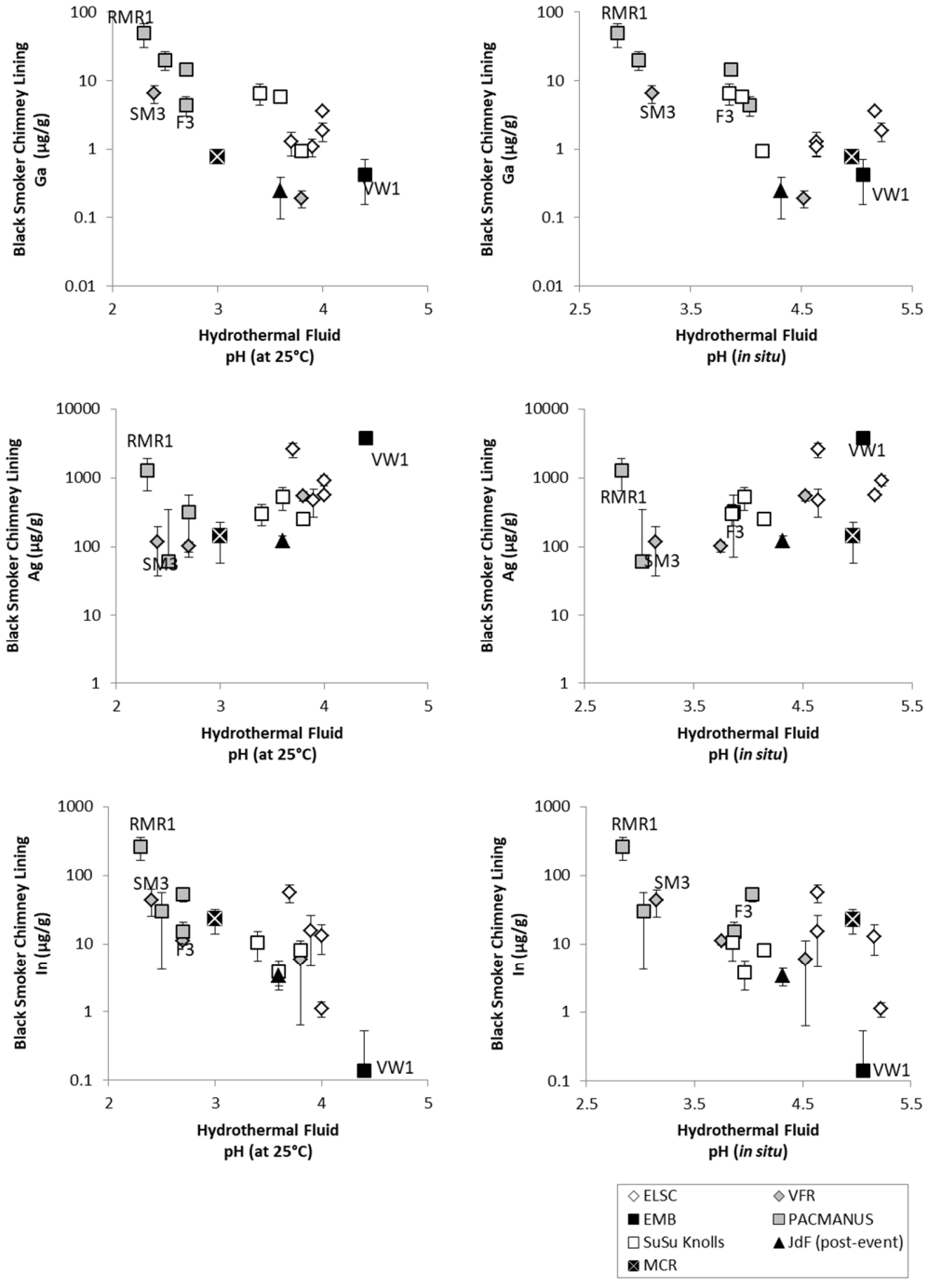

Figure 10. Thermodynamic stability diagrams from Wood and Samson (2006) showing pH vs. the log concentration of aqueous Ga complexes contributing to the solubility of GaOOH at 300°C at vapor saturated pressures using the thermodynamic data of Benézéth et al. (1997) and pH vs. the log concentration of aqueous In complexes contributing to the solubility of In_2S_3 at 20°C and 1M $NaClO_4$, total S = 0.01M using thermodynamic data from Tunaboylu and Schwarzenbach (1970). Red lines highlight the activities of free ions, Ga^{3+} and In^{3+}, as a function of pH.

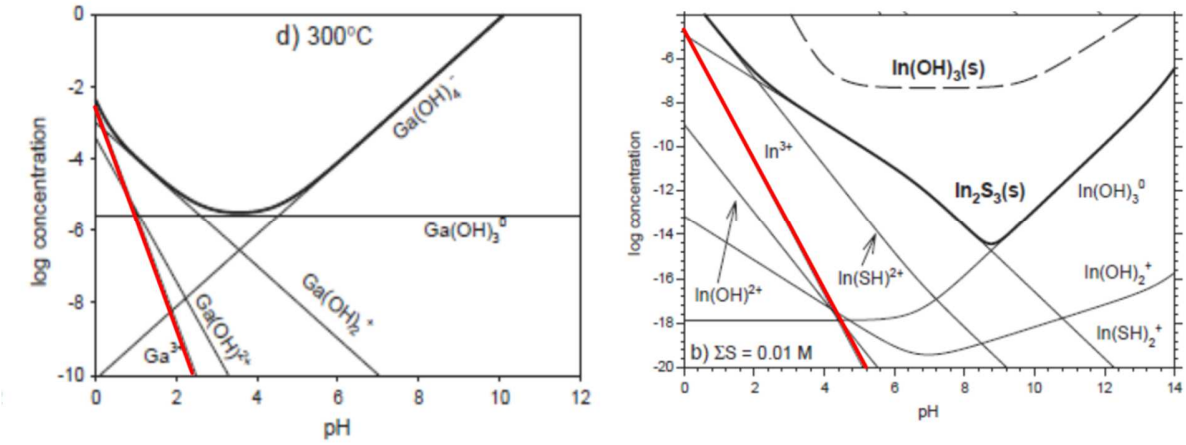

Figure 11. Free ion activity ratios {Co^{2+} }:{ Fe^{2+}} and {Ni^{2+} }:{ Fe^{2+}} in hydrothermal fluids as calculated by EQ3/6 vs. Co and Ni concentrations in in paired black smoker chimney linings.. Also shown are total Co:Fe and Ni:Fe concentration ratios vs. Co and Ni concentrations in in paired black smoker chimney linings. X-axes cross at SIMS detection limits. ELSC = Eastern Lau Spreading Center, VFR = Valu Fa Ridge; EMB = Eastern Manus Basin; JdF = Juan de Fuca Ridge; MCR = Mid-Cayman Rise. Fluid data sources are: Eastern Lau Spreading Center (Seewald, 2017; this paper), Manus Basin (Craddock,2009), Main Endeavour Field (Seyfried et al.,2003), Mid-Cayman Rise (McDermott et al., 2018).

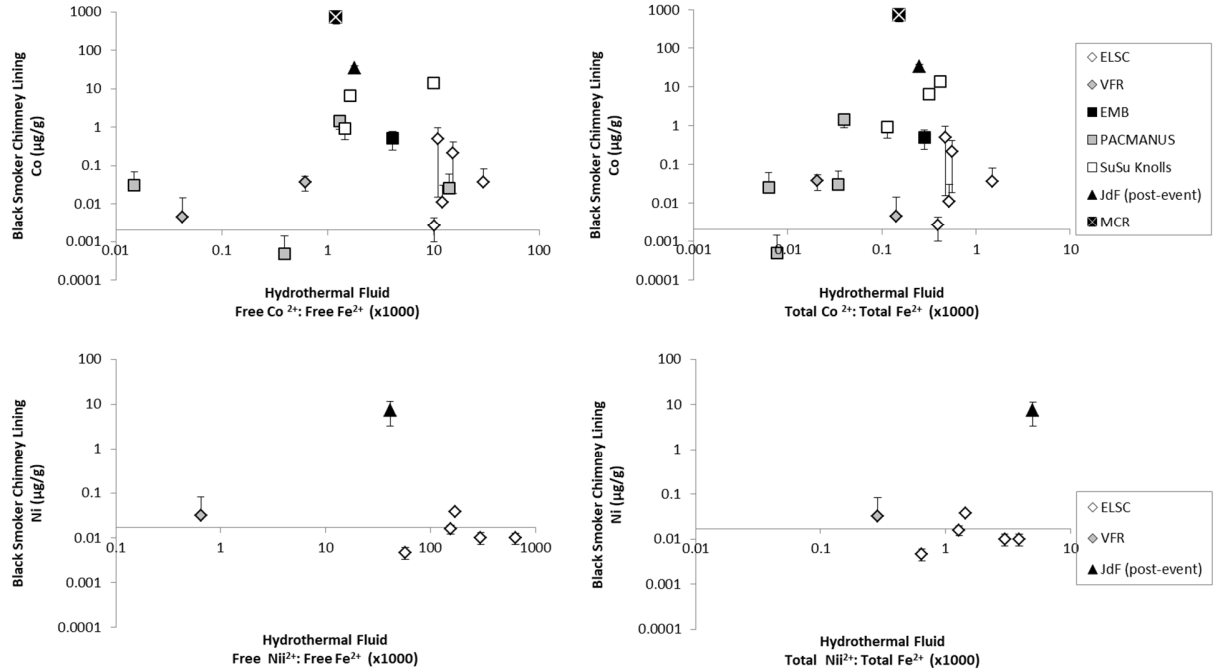

Table 1.

Vent Fluid and Black Smoker Chimney Sample Information. Samples in bold were used to generate callibration curves for secondary ion mass spectrometry (SIMS). References for lithology are: (a) Krasnov et al. (1997); (b) Karsten et al. (1990); (c) Langmuir et al. (1997); (d) Elthon et al. (1995); (e) Sinton et al. (2003); (f) Binns and Scott (1993); Kamenetsky et al. (2001); Sinton et al. (2003); (g) Jenner et al. (1987); Frenzel et al. (1990); Vallier et al. (1991); Fouquet et al. (1993); Martinez and Taylor (2002); Langmuir et al. (2006); Bézos et al. (2009); Escrig et al. (2009). References for fluid chemistry are: (h) O'Grady (2001); (i) Seyfried et al. (2003); (j) McDermott et al. (2018); (k) Reeves et al. (2011); (l) Mottl et al. (2011); (m) Seewald (2017); (n) This Paper. Data from this paper are underlined. E-MORB = enriched mid-ocean ridge basalt; cp = chalcopyrite; cb = cubanite; cp/wz = intergrown chalcopyrite and wurtzite; cp/py = intergrown chalcopyrite and pyrite; mm = mmol/kg vent fluid; µm = µmol/kg vent fluid; nm = nmol/kg vent fluid.

Region, Lithology Vent Field	Year	Chimney Sample	Lining Mineral	Vent Fluid		Temp. (°C)	pH (25°C)	Cl mm	H_2S mm	Fe µm	Cu µm	Co nm	Ni nm	Ga nm	Ag nm	In nm
Southern East Pacific Rise, basalt[a]																
17°34'S	**1998**	**Alv3299-6-1**	**cp**	**Hobbes**												
17°37'S	1998	Alv3288-5-1a	cp	Simon		337	3.4	751	3.5	5300	51					
17°37'S	1998	Alv3296-2-2a	cp	Maggie												
17°37'S	**1998**	**Alv3296-3**	**cp**	**Wally**												
17°37'S	1998	Alv3296-5-1a	cp	Homer												
Juan de Fuca Ridge, basalt[b]																
MEF	**1987**	**Alv1931**	**cp**	**none**												
MEF	**1999**	**Alv3474-3-1**	**cp**	**Sully99**	[h]	**379**	**3.6**	**39**	**20**	**400**	**12**	**100**	**2000**		**4**	
MEF	1999	Alv3480-4	cp	none												
Mid-Atlantic Ridge, E-MORB[c]																
Lucky Strike	1994	DV1-5B	cp	none												
Mid-Cayman Rise, basalt[d]																
Beebe / I	2013	J2-613-16-R1	cb	BB5	[i]	395	3	351	0.01	6500	172	1000				
Manus Spreading Center, basalt[e]																
Vienna V	2006	J2-207-1-R1	cp/wz	VW1	[j]	282	4.4	691	1.4	159	4	45			38	
Eastern Manus Basin (PACMANUS), felsic[f]																
Fenway	2006	J2-210-7-R2	cp	none												
Fenway	2006	J2-216-16-R1	cp	F3	[j]	358	2.7	562	18.8	12950	138	517			290	
Satanic M	2006	J2-214-3-R1	cp	SM3	[j]	288	2.5	503	10.2	1298	140	10			75	
Roman R	2006	J2-208-1-R1	cp	RMR1	[j]	314	2.3	632	7.5	6731	165	234			720	
Roger's R	2006	J2-213-6-R1	cp	RGR1	[j]	320	2.7	648	3.6	4610	213	29			223	
Eastern Manus Basin (Susu Knolls), felsic[f]																
Suzette	2006	J2-217-2-R1	cp	SZ1	[j]	303	3.8	626	1.8	720	53	230			35	
Suzette	2006	J2-217-10-R1	cp	SZ2	[j]	274	3.6	684	1.8	880	27	101			60	
Suzette	2006	J2-219-2-R1	cp	none												
North Su	2006	J2-223-1-R1	cp	NS3	[j]	300	3.4	673	3.4	2390	108	1003			52	
North Su	2006	J2-227-10-R1	cp	none												
Eastern Lau Spreading Center, felsic[g]																
Tahi Moa	2009	J2-450-3-R1	cp/wz	TMo5	[k,m]	310	3.7	555	3.3	278	6	115	361	2	26	
ABE	2009	J2-449-6-R1	cp/py	A10	[k,m]	317	3.9	543	3.9	168	10	80	108	10	14	
ABE	2009	J2-449-5-R1	cp/wz	A11	[k,m]	306	4.0	552	2.7	139	9	73	178	6	6	
ABE	2015	J2-815-5-R1	cp/wz	A16	[l,m]	300	4.0	546	3.7	67	4	98	200	62	0	40
Valu Fa Ridge, felsic[g]																
Tu'i Mali	2009	J2-442-4-R2	cp/py	TM11	[k,m]	315	3.8	653	2.8	184	20	96	693	6	19	
Tu'i Mali	2015	J2-819-4-R2	cp/wz	TM15	[l,m]	269	3.9	598	2.3				886			
Mariner	**2009**	**J2-437-3-R2**	**cp**	**MA9**	**[k,m]**	**338**	**2.3**	**541**	**8.9**	**14147**	**300**	**201**	**402**	**118**	**66**	
Mariner	**2015**	**J2-817-4-R2**	**cp**	**MA15**	**[l,m]**	**354**	**3.0**	**557**	**3.1**	**12464**	**238**	**261**	**315**	**175**	**56**	**94**

mm = mmol/kg; µm = µmol/kg; nm = nmol/kg; E-MORB = enriched mid-ocean ridge basalt; cp = chalcopyrite; cb = cubanite; cp/wz = intergrown chalcopyrite and wurtzite; cp/py = intergrown chalcopyrite and pyrite. References for lithology are: (a) Krasnov et al. (1997); (b) Karsten et al. (1990); (c) Langmuir et al. (1997); (d) Elthon et al. (1995); (e) Sinton et al. (2003); (f) Binns and Scott (1993); Kamenetsky et al. (2001); Sinton et al. (2003); (g) Jenner et al. (1987); Frenzel et al. (1990); Vallier et al. (1991); Fouquet et al. (1993); Martinez and Taylor (2002); Langmuir et al. (2006); Bézos et al. (2009); Escrig et al. (2009). References for fluid chemistry are: (h) O'Grady (2001); (i) Seyfried et al. (2003); (j) McDermott et al. (2018); (k) Reeves et al. (2011); (l) Mottl et al. (2011); (m) Seewald (2017); (n) This Paper. Data from this paper are underlined. Samples in bold were used to generate callibration curves for secondary ion mass spectrometry (SIMS).

Table 2.

Machine settings, typical secondary ion intensities, and associated errors for secondary ion mass spectrometry (SIMS) analyses of Co, Ni, Ga, Ag, and In in chalcopyrite. cps = counts per second.

Source	duoplasmatron O_2-
Primary Beam Current	10 nA
Secondary Accelerating Voltage	10 kV
Energy Offset	none
Field Aperture	22 x 22 µm
Raster Area	20 x 20 µm
Spot Diameter	40 µm
Mass Resolving Power	~10,000
Number of Cycles	10
Pre-sputter time	300 s
Integration Time, Trace elements and background	10 s
Integration Time ($^{63}Cu^{16}O^+$, $^{54}Fe^{16}O+$, $^{64}Zn^{16}O+$)	5 s
Secondary Ion Intensity on $^{63}Cu^{16}O^+$ (1000 cps)	5 to 10
Relative Standard Deviation of Ion Intensity on $^{63}Cu^{16}O^+$	10%
Counting Errors on $^{63}Cu^{16}O^+$ (%)	0.50%
Secondary Ion Intensity on background mass 54.7 (cps)	< 0.1
Detection Limit (background + 3 × standard deviation)	0.25 cps (5×10^{-5} cps / $^{63}Cu^{16}O^+$ cps)
Determination Limit (background + 10 × standard deviation)	0.6 cps (1.2×10^{-4} cps / $^{63}Cu^{16}O^+$ cps)

Table 3.

Inputs (vent fluid temperature, pH (at 25°C), and major element concentrations) and outputs (in situ pH, fO2, and fS2) of EQ3/6 thermodynamic modeling for vent fluid pairs of black smoker chimney linings analyzed by SIMS. Data for vent fluids from the Eastern Lau Spreading Center and Valu Fa Ridge are from Seewald (2017), Evans et al. (2017), and this paper. Data for vent fluids in the Manus Basin are from Craddock (2009) and Reeves et al. (2011), data for fluid Sully99 from the Main Endeavour Field are from Seyfried et al. (2003), and data for fluid BB5 from the Beebe / Piccard vent field are from McDermott (2015). µM = µmol / L vent fluid; mm = mmol / kg vent fluid; µm = µmol / kg vent fluid.

Vent Field	Vent Fluid	Temp. (°C)	pH (at 25°C)	Cl mm	Na mm	Ca mm	K mm	Mn µm	Fe µm	H_2S mm	H_2 µM	pH *in situ* (calculated)	log fO_2	log fS_2
Eastern Lau Spreading Center														
Tahi Moana-1	TMo5	310	3.7	555	405	64.4	19.2	400	280	3.3	114	4.6	-31.7	-10.0
ABE	A10	317	3.9	543	437	40.3	24.6	440	170	3.9	63	4.6	-31.6	-9.5
ABE	A11	306	4.0	552	446	40.2	24.9	380	140	2.7	114	5.2	-32.1	-10.3
ABE	A16	300	4.0	552	449	38.4	25.6	260	67	3.0	114	5.2	-32.7	-10.4
Valu Fa Ridge														
Tu'i Malila	TM11	315	3.8	652	510	48.7	43.0	380	180	2.8	418	4.5	-32.4	-11.1
Mariner	MA9	338	2.4	470	313	43.4	28.3	5200	12500	8.9	414	3.2	-30.2	-9.3
Mariner	MA15	354	2.7	521	370	41.7	30.1	4400	12500	10.0	78	3.8	-27.4	-7.3
Manus Spreading Center														
Vienna Woods	VW1	282	4.4	691	509	80.1	21.2	350	150	1.4	43	5.1	-33.7	-10.9
Eastern Manus Basin (PACMANUS)														
Roger's Ruins	RGR1	320	2.7	648	489	27.1	81.1	3000	6900	3.6	20	4.0	-30.5	-9.4
Roman Ruins	RMR1	314	2.3	632	482	19.8	81.7	4000	5600	7.5	76	2.8	-29.9	-8.3
Satanic Mills	SM3	288	2.7	503	398	13.7	68.0	2300	1200	10.2	8	3.0	-31.7	-7.5
Fenway	F3	358	2.7	562	407	22.3	76.1	3800	11800	18.8	407	3.9	-28.5	-8.1
Eastern Manus Basin (SuSu Knolls)														
North Su	NS3	300	3.4	673	541	30.6	65.0	430	2300	3.4	82	3.9	-32.5	-10.0
Suzette	SZ1	303	3.8	626	508	33.8	48.0	270	750	1.8	12	4.1	-35.7	-10.6
Suzette	SZ2	274	3.6	684	533	49.4	49.2	370	780	1.8	7	4.0	-33.0	-9.4
Juan de Fuca Ridge														
Main Endeavour Field	Sully99	379	3.6	39	32	1.9	2.0	90	400	20.0	960	4.3	-28.0	-8.7
Mid-Cayman Rise														
Beebe/Piccard	BB5	395	3.0	352	313	6.1	11.5	560	6500	12.3	19200	5.0	-28.7	-10.7

Table 4.

Results of SIMS analyses. n = number of spots on each sample; Gray text indicates value below quantitative determination limit; NM = not measured; bdl = below detection limit; none = no vent fluid pair.

Region			59Co/63Cu16O		60Ni/63Cu16O		69Ga/63Cu16O		109Ag/63Cu16O		115In/63Cu16O	
Vent Field, Chimney Sample, Vent Fluid			n	Average ± 1σ	n	Average ± 1σ	n	Average ± 1σ	n	Average ± 1σ	n	Average ± 1σ
Detection Limit = 5E-05												
Quantitative Determination Limit = 1.2E-04												
Southern East Pacific Rise												
17°34'S	Alv3299-6-1	Hobbes	31	3.3E+00 ± 4.1E-01	31	3.0E-01 ± 2.0E-02	31	3.2E-02 ± 5.0E-03	31	2.3E-02 ± 3.2E-03	31	8.1E-01 ± 2.1E-01
17°37'S	Alv3288-5-1a	Simon	7	1.1E+00 ± 1.3E-01	7	3.1E-02 ± 1.3E-03	7	2.4E-02 ± 9.4E-03	7	5.4E-03 ± 6.4E-04	7	3.1E-01 ± 9.5E-02
17°37'S	Alv3296-2-2a	Maggie	14	1.9E+00 ± 2.9E-01	14	1.1E-01 ± 1.6E-02	14	1.4E-02 ± 3.1E-03	14	4.5E-03 ± 1.0E-03	14	1.4E-01 ± 4.9E-02
17°37'S	Alv3296-3	Wally	12	7.4E-01 ± 6.8E-02	12	8.4E-02 ± 3.3E-03	12	7.4E-02 ± 3.1E-02	12	6.6E-02 ± 1.3E-02	12	1.5E+00 ± 4.9E-01
17°37'S	Alv3296-5-1a	Homer	8	2.0E+00 ± 6.7E-02	8	1.2E-01 ± 4.7E-03	8	1.2E-02 ± 1.2E-03	8	4.4E-03 ± 2.3E-04	8	1.5E-01 ± 7.8E-03
Juan de Fuca Ridge												
MEF	Alv1931	none	12	6.2E-05 ± 1.4E-05	12	1.9E-04 ± 3.4E-05	12	5.0E-02 ± 1.0E-02	12	5.9E-03 ± 3.2E-04	12	1.4E+00 ± 8.7E-02
MEF	Alv3474-3-1	Sully99	27	8.2E-01 ± 1.2E-01	8	2.3E-02 ± 1.2E-02	8	1.3E-02 ± 7.9E-03	27	3.1E-03 ± 5.6E-04	27	3.2E-01 ± 9.1E-02
MEF	Alv3480-4	none	6	8.0E-01 ± 8.9E-02		NM		NM	6	2.7E-03 ± 4.6E-04	6	3.5E-01 ± 3.4E-02
Mid-Atlantic Ridge												
Lucky Strike	DV1-5B	none	5	6.1E-01 ± 7.4E-02		NM		NM	5	4.8E-02 ± 2.1E-02	5	1.7E+00 ± 2.4E-01
Mid-Cayman Rise												
Beebe/Piccard	J2-613-16-R1	BB5	19	1.7E+01 ± 5.8E+00	3	1.3E+00 ± 6.6E-02	3	4.1E-02 ± 1.9E-03	19	3.6E-03 ± 2.2E-03	19	2.2E+00 ± 8.6E-01
Manus Spreading Center												
Vienna Woods	J2-207-1-R1	VW1	88	1.2E-02 ± 6.1E-03	21	5.6E-05 ± 2.0E-05	21	2.3E-02 ± 1.5E-02	88	9.6E-02 ± 1.6E-02	88	1.3E-02 ± 3.7E-02
Eastern Manus Basin (PACMANUS)												
Fenway	J2-210-7-R2	none	7	7.1E-05 ± 4.2E-05		NM		NM	7	4.3E-03 ± 1.4E-03	7	2.6E+00 ± 9.3E-01
Fenway	J2-216-16-R1	F3	13	3.4E-02 ± 1.3E-02	3	7.1E-04 ± 2.2E-04	3	7.7E-01 ± 8.0E-02	13	8.1E-03 ± 6.3E-03	8	1.4E+00 ± 5.2E-01
Satanic Mills	J2-214-3-R1	SM3	27	bdl	8	1.7E-04 ± 6.0E-05	8	1.1E+00 ± 3.3E-01	27	1.5E-03 ± 7.4E-03	27	2.8E+00 ± 2.4E+00
Roman Ruins	J2-208-1-R1	RMR1	24	7.3E-04 ± 9.1E-04	6	1.2E-04 ± 2.3E-05	6	2.6E+00 ± 9.9E-01	24	3.3E-02 ± 1.6E-02	11	2.5E+01 ± 9.0E+00
Roger's Ruins	J2-213-6-R1	RGR1	13	bdl	6	bdl	6	2.4E-01 ± 1.6E-01	13	6.6E-03 ± 7.6E-04	13	4.9E+00 ± 1.1E+00
Eastern Manus Basin (SuSu Knolls)												
Suzette	J2-217-2-R1	SZ1	13	1.6E-01 ± 2.3E-02	3	5.6E-03 ± 2.3E-04	3	5.1E-02 ± 1.1E-02	13	6.4E-03 ± 1.1E-03	8	7.7E-01 ± 1.1E-01
Suzette	J2-217-10-R1	SZ2	20	2.2E-02 ± 1.0E-02	3	1.1E-03 ± 1.5E-04	3	3.1E-01 ± 5.3E-02	20	1.3E-02 ± 5.0E-03	9	3.6E-01 ± 1.7E-01
Suzette	J2-219-2-R1	none	5	2.1E-04 ± 1.2E-04		NM		NM	5	9.2E-03 ± 3.8E-03	5	1.0E+00 ± 5.3E-01
North Su	J2-223-1-R1	NS3	21	3.3E-01 ± 1.0E-01	7	1.8E-02 ± 3.9E-03	7	3.6E-01 ± 1.2E-01	21	7.7E-03 ± 2.6E-03	17	9.8E-01 ± 4.5E-01
North Su	J2-227-10-R1	none	10	8.8E-03 ± 1.5E-03		NM		NM	10	5.4E-03 ± 8.6E-04	10	1.0E+00 ± 4.5E-01
Eastern Lau Spreading Center												
Tahi Moana-1	J2-450-3-R1	TMo5	18	6.4E-05 ± 4.0E-05	3	1.2E-04 ± 9.2E-06	3	6.9E-02 ± 2.6E-02	18	6.6E-02 ± 1.6E-02	18	5.3E+00 ± 1.5E+00
ABE	J2-449-5-R1	A10	20	2.6E-04 ± 4.7E-04	8	bdl	8	1.0E-01 ± 3.1E-02	20	2.3E-02 ± 4.1E-03	20	1.0E-01 ± 2.5E-02
ABE	J2-449-6-R1	A11	22	1.2E-02 ± 1.1E-02	6	bdl	6	5.8E-02 ± 1.6E-02	22	1.2E-02 ± 5.3E-03	22	1.4E+00 ± 1.0E+00
ABE	J2-815-5-R1	A16	9	8.8E-04 ± 1.1E-03	3	bdl	3	1.9E-01 ± 1.5E-02	9	1.4E-02 ± 1.9E-03	9	1.2E+00 ± 5.7E-01
Valu Fa Ridge												
Tu'i Malila	J2-442-4-R2	TM11	17	5.2E-03 ± 4.7E-03	3	bdl	3	1.0E-02 ± 2.9E-03	17	1.4E-02 ± 2.1E-03	17	5.6E-01 ± 5.0E-01
Tu'i Malila	J2-819-4-R2	TM15	4	1.8E-04 ± 8.2E-05		NM		NM	4	5.4E-02 ± 6.4E-03	4	3.8E-02 ± 8.1E-03
Mariner	J2-437-3-R2	MA9	12	1.1E-04 ± 2.4E-04	6	9.9E-05 ± 1.5E-04	6	3.5E-01 ± 1.0E-01	12	2.9E-03 ± 2.0E-03	12	4.1E+00 ± 1.7E+00
Mariner	J2-817-4-R2	MA15	6	8.9E-04 ± 3.9E-04		NM		NM	6	2.6E-03 ± 4.3E-04	6	1.0E+00 ± 1.2E-01

Table 5.

Calculated concentrations of trace elements in chalcopyrite lining black smoker chimneys based on SIMS measurements and calibration curves. bdl = below

Region	Chimney	Vent	Co	Ni	Ga	Ag	In
Vent Field	Sample	Fluid	µg/g	µg/g	µg/g	µg/g	µg/g
	Detection Limit =		2 ng/g	17 ng/g	0.9 ng/g	2 µg/g	0.5 ng/g
	Determination Limit =		5 ng/g	40 ng/g	2 ng/g	5 µg/g	1.2 ng/g
Southern East Pacific Rise							
17°34'S	**Alv3299-6-1**	**Hobbes**	**147 ± 18**	**99 ± 7**	**bdl**	**890 ± 120**	**8.8 ± 2.3**
17°37'S	Alv3288-5-1a	Simon	47 ± 6	10 ± 0.4	bdl	211 ± 25	3.4 ± 1.0
17°37'S	Alv3296-2-2a	Maggie	81 ± 13	37 ± 5	bdl	180 ± 40	1.5 ± 0.5
17°37'S	**Alv3296-3**	**Wally**	**32 ± 3**	**28 ± 1**	**1.4 ± 0.6**	**2600 ± 500**	**16 ± 5**
17°37'S	Alv3296-5-1a	Homer	86 ± 3	39 ± 2	bdl	174 ± 9	1.57 ± 0.08
Juan de Fuca Ridge							
MEF	**Alv1931**	**none**	**2.7 ng/g ± 0.6 ng/g**	**66 ng/g ± 12 ng/g**	**0.9 ± 0.2**	**232 ± 12**	**15.6 ± 0.9**
MEF	**Alv3474-3-1**	**Sully99**	**36 ± 5**	**7.6 ± 4.2**	**bdl**	**121 ± 22**	**3.4 ± 1.0**
MEF	Alv3480-4	none	35 ± 4	NM	NM	106 ± 18	3.7 ± 0.4
Mid-Atlantic Ridge							
Lucky Strike	DV1-5B	none	27 ± 3	NM	NM	1900 ± 800	18 ± 3
Mid-Cayman Rise							
Beebe/Piccard	J2-613-16-R1	BB5	760 ± 250	454 ± 22	bdl	140 ± 90	23 ± 9
Manus Spreading Center							
Vienna Woods	J2-207-1-R1	VW1	0.53 ± 0.27	19 ng/g ± 7 ng/g	bdl	3800 ± 700	bdl
Eastern Manus Basin (PACMANUS)							
Fenway	J2-210-7-R2	none	3.1 ng/g ± 3.1 ng/g	NM	NM	170 ± 60	28 ± 10
Fenway	J2-216-16-R1	F3	1.5 ± 0.6	0.24 ± 0.07	NM	320 ± 250	15 ± 6
Satanic Mills	J2-214-3-R1	SM3	bdl	56 ng/g ± 20 ng/g	20 ± 6	60 ± 60	31 ± 26
Roman Ruins	J2-208-1-R1	RMR1	32 ng/g ± 40 ng/g	42 ng/g ± 8 ng/g	48 ± 18	1300 ± 600	270 ± 100
Roger's Ruins	**J2-213-6-R1**	**RGR1**	**bdl**	**bdl**	**4.4 ± 2.9**	**260 ± 30**	**53 ± 12**
Eastern Manus Basin (SuSu Knolls)							
Suzette	J2-217-2-R1	SZ1	6.9 ± 1.0	1.9 ± 0.1	bdl	250 ± 40	8.3 ± 1.2
Suzette	J2-217-10-R1	SZ2	1.0 ± 0.5	0.36 ± 0.05	5.8 ± 1.0	530 ± 200	3.9 ± 1.8
Suzette	J2-219-2-R1	none	9 ng/g ± 5 ng/g	NM	NM	360 ± 150	11 ± 6
North Su	J2-223-1-R1	NS3	15 ± 4	6.2 ± 1.3	6.5 ± 2.2	300 ± 100	11 ± 5
North Su	J2-227-10-R1	none	0.38 ± 0.07	NM	NM	210 ± 30	11 ± 5
Eastern Lau Spreading Center							
Tahi Moana-1	J2-450-3-R1	TMo5	2.8 ng/g ± 1.7 ng/g	40 ng/g ± 3 ng/g	1.3 ± 0.5	2600 ± 600	57 ± 17
ABE	J2-449-5-R1	A10	12 ng/g ± 20 ng/g	bdl	1.8 ± 0.6	920 ± 160	1.1 ± 0.3
ABE	J2-449-6-R1	A11	0.5 ± 0.5	bdl	1.1 ± 0.3	470 ± 210	16 ± 11
ABE	J2-815-5-R1	A16	39 ng/g ± 47 ng/g	bdl	3.5 ± 0.3	570 ± 70	13 ± 6
Valu Fa Ridge							
Tu'i Malila	J2-442-4-R2	TM11	0.2 ± 0.2	bdl	bdl	540 ± 80	6 ± 5
Tu'i Malila	J2-819-4-R2	TM15	8 ng/g ± 4 ng/g	NM	NM	2110 ± 250	bdl
Mariner	**J2-437-3-R2**	**MA9**	**5 ng/g ± 11 ng/g**	**33 ng/g ± 52 ng/g**	**6.4 ± 1.9**	**120 ± 80**	**44 ± 19**
Mariner	J2-817-4-R2	MA15	39 ng/g ± 17 ng/g	NM	NM	100 ± 20	11.2 ± 1.3

Table 6.

Concentrations of major elements and recovered mass in picks of chalcopyrite black smoker chimney linings obtained by inductively

Chimney Sample	Vent Field	Tarnish Condition	Mass mg	otal Recover wt%	Cu wt%	Fe wt%	Zn wt%	S wt%	Ca wt%	Ba µg/g	Si wt%
Alv3296-3 pick A1	17°37'S	minor	11.88 ± 0.05	86 ± 6	32 ± 3	40 ± 5	0.17 ± 0.05	28 ± 3	1.5 ± 0.6	bdl	0.2 ± 0.1
Alv3296-3 pick A2		minor	8.81 ± 0.02	96 ± 5	28 ± 2	35 ± 4	0.13 ± 0.04	37 ± 3	0.2 ± 0.6	bdl	0.2 ± 0.1
Alv3296-3 pick B1		minor	14.63 ± 0.03	89 ± 5	30 ± 2	36 ± 5	0.13 ± 0.05	34 ± 3	0.2 ± 0.6	bdl	0.2 ± 0.1
Alv3296-3 pick B2		minor	13.04 ± 0.03	95 ± 6	35 ± 3	35 ± 5	0.12 ± 0.04	30 ± 3	0.2 ± 0.6	bdl	0.2 ± 0.1
Alv3299-6-1 pick A	17°34'S	none	20.01 ± 0.03	90 ± 5	31 ± 2	38 ± 4	0.44 ± 0.05	31 ± 3	0.2 ± 0.6	bdl	0.1 ± 0.1
Alv3299-6-1 pick B1		none	7.75 ± 0.08	95 ± 6	30 ± 2	37 ± 5	0.37 ± 0.22	33 ± 3	0.1 ± 0.6	bdl	0.2 ± 0.1
Alv3299-6-1 pick B2		none	10.07 ± 0.03	93 ± 5	27 ± 2	35 ± 5	0.07 ± 0.04	38 ± 3	0.1 ± 0.6	bdl	0.1 ± 0.1
Alv3299-6-1 pick C		none	4.60 ± 0.04	99 ± 6	30 ± 2	37 ± 5	0.7 ± 0.3	32 ± 3	0.1 ± 0.7	bdl	0.1 ± 0.2
Alv1931 pick A1	MEF	none	3.68 ± 0.05	106 ± 7	31 ± 2	36 ± 5	0.3 ± 0.3	33 ± 3	0.2 ± 0.7	bdl	0.1 ± 0.2
Alv1931 pick A2		none	5.10 ± 0.10	95 ± 6	29 ± 2	34 ± 5	0.09 ± 0.03	37 ± 3	0.2 ± 0.6	bdl	0.2 ± 0.1
Alv1931 pick A3		none	16.02 ± 0.03	63 ± 3	31 ± 2	36 ± 3	0.07 ± 0.03	34 ± 2	0.1 ± 0.3	13 ± 39	0.1 ± 0.1
Alv3474-3-1 pick A1	MEF	none	10.5 ± 0.4	99 ± 5	28 ± 2	42 ± 4	bdl	30 ± 3	0.1 ± 0.6	bdl	0.2 ± 0.1
Alv3474-3-1 pick A2		none	15.25 ± 0.04	91 ± 5	30 ± 2	36 ± 5	bdl	35 ± 3	0.1 ± 0.6	bdl	0.2 ± 0.1
Alv3474-3-1 pick A3		none	11.17 ± 0.04	108 ± 5	25 ± 2	48 ± 4	bdl	27 ± 2	0.1 ± 0.6	bdl	0.2 ± 0.1
J2-213-6-R1 pick A	Roger's Ruins	minor	18.54 ± 0.06	90 ± 5	30 ± 2	36 ± 5	bdl	33 ± 3	0.2 ± 0.6	bdl	0.2 ± 0.1
J2-214-3-R1 pick A		tarnish	6.76 ± 0.04	90 ± 5	30 ± 2	36 ± 5	bdl	34 ± 3	0.1 ± 0.6	bdl	0.2 ± 0.1
J2-214-3-R1 pick C	Satanic Mills	tarnish	4.78 ± 0.10	97 ± 5	31 ± 2	35 ± 4	1.0 ± 0.3	34 ± 3	0.1 ± 0.6	24 ± 91	0.1 ± 0.1
J2-437-3-R2 pick A	Mariner	minor	2.0 ± 0.20	90 ± 5	29 ± 2	40 ± 5	0.04 ± 0.01	31 ± 3	0.1 ± 0.6	172 ± 89	0.2 ± 0.1

Table 7.

Concentrations of trace elements in picks of chalcopyrite black smoker chimney linings obtained by inductively coupled plasma

Chimney Sample	Vent Field	Co µg/g	Ni µg/g	Ga µg/g	Ag µg/g	In µg/g
Alv3296-3 pick A1	17°37'S	41 ± 4	50 ± 23	1.43 ± 0.03	2700 ± 170	20.7 ± 2.3
Alv3296-3 pick A2		35 ± 3	40 ± 21	1.24 ± 0.02	2500 ± 160	16.3 ± 1.9
Alv3296-3 pick B1		38 ± 3	40 ± 22	1.38 ± 0.02	2900 ± 180	17.2 ± 2.0
Alv3296-3 pick B2		30 ± 3	40 ± 21	1.07 ± 0.04	2300 ± 140	15.9 ± 1.9
Alv3299-6-1 pick A	17°34'S	150 ± 13	110 ± 26	0.67 ± 0.08	490 ± 30	6.7 ± 1.3
Alv3299-6-1 pick B1		140 ± 12	110 ± 25	0.56 ± 0.08	880 ± 60	6.4 ± 1.2
Alv3299-6-1 pick B2		130 ± 11	120 ± 24	0.53 ± 0.07	850 ± 60	9.1 ± 1.4
Alv3299-6-1 pick C		150 ± 13	110 ± 26	0.56 ± 0.08	660 ± 40	6.8 ± 1.3
Alv1931 pick A1	MEF	bdl	40 ± 22	1.07 ± 0.05	270 ± 20	10.5 ± 1.5
Alv1931 pick A2		0.73 ± 0.24	bdl	0.93 ± 0.05	270 ± 14	20.0 ± 1.5
Alv1931 pick A3		0.80 ± 0.23	bdl	1.19 ± 0.01	290 ± 20	17.5 ± 1.8
Alv3474-3-1 pick A1	MEF	46 ± 4	bdl	0.34 ± 0.08	130 ± 11	6.2 ± 1.1
Alv3474-3-1 pick A2		48 ± 4	bdl	0.49 ± 0.08	150 ± 12	6.6 ± 1.2
Alv3474-3-1 pick A3		42 ± 4	bdl	0.37 ± 0.07	130 ± 10	5.9 ± 1.1
J2-213-6-R1 pick A	Roger's Ruins	0.7 ± 0.3	30 ± 21	3.3 ± 0.10	330 ± 23	37 ± 4
J2-214-3-R1 pick A		0.5 ± 0.3	bdl	40.4 ± 2.5	140 ± 11	77 ± 6
J2-214-3-R1 pick C	Satanic Mills	0.32 ± 0.28	bdl	23.7 ± 1.4	100 ± 9	45 ± 4
J2-437-3-R2 pick A	Mariner	0.54 ± 0.10	bdl	6.40 ± 0.09	137 ± 4	36.4 ± 1.2

Table 8.

Endmember Metal Concentrations of Hydrothermal Vent Fluids from the Eastern Lau Spreading Center and Valu Fa Ridge

Fluid	n =	min. Mg	max. T	min. pH	Cr	Mn	Fe	Co	Ni	Cu	Zn	Ga
		mm	°C	(25°C)	nm	µm	µm	nm	nm	µm	µm	nm
TMo1	2	2.4	306	3.3	1100 ± NM	580 ± 2	370 ± 30	146 ± 6	700 ± 140	8 ± NM	220 ± 27	15 ± 4
TMo2	2	1.0	298	3.9	1180 ± 50	293 ± 1	248 ± 3	160 ± 28	200 ± 140	8 ± 1	120 ± 50	10 ± 8
TMo5	2	1.4	310	3.7	630 ± 24	396 ± 5	278 ± 7	110 ± 8	400 ± 300	6 ± 0	83 ± 0	2 ± 0
A10	1	2.1	317	4.4	4400 ± NM	440 ± NM	170 ± NM	80 ± NM	110 ± NM	10 ± NM	100 ± NM	10 ± NM
A11	2	2.1	312	3.9	740 ± NM	400 ± 90	140 ± 30	73 ± 1	180 ± 50	9 ± 3	80 ± 0	6 ± 2
A13	2	2.3	283	4.3	1400 ± NM	450 ± 28	200 ± NM	115 ± 6	570 ± NM	5 ± NM	110 ± NM	110 ± NM
A14	2	1.9	300	4.0	1500 ± NM	400 ± 24	340 ± NM	180 ± 18	400 ± NM	75 ± NM	430 ± NM	83 ± NM
A15	2	1.9	290	4.4	1400 ± 260	240 ± 27	120 ± 4	130 ± 30	500 ± 90	9 ± 0	80 ± 20	73 ± 6
A16	2	1.7	263	4.5	700 ± 240	258 ± 3	67 ± 3	100 ± 40	200 ± 60	4 ± 1	37 ± 1	62 ± 3
TM11	2	1.1	315	3.8	3000 ± 1700	376 ± 1	180 ± 8	100 ± 15	700 ± 200	20 ± NM	110 ± 16	6 ± 4
TM12	2	3.0	284	4.2	7900 ± 400	350 ± 4	280 ± 22	117 ± 1	210 ± 22	25 ± 1	200 ± 110	50 ± 40
TM13	2	3.6	262	3.9	309 ± 7	296 ± 1	102 ± 3	167 ± 6	110 ± 50	9 ± 0	85 ± 4	66 ± 7
TM14	2	1.5	290	3.9	360 ± 40	300 ± 80	150 ± 30	200 ± 50	77 ± 5	7 ± 0.03	91 ± 1	80 ± 22
TM15	1	22.0	269	5.0	1500 ± NM	370 ± NM	cont. ± NM	cont ± NM	890 ± NM	cont ± NM	cont ± NM	cont ± NM
TM16	2	5.5	251	3.9	370 ± 50	410 ± 19	500 ± 140	180 ± 8	76 ± 3	12 ± 6	960 ± NM	80 ± 11
TM17	2	3.1	258	3.9	500 ± 190	280 ± 8	400 ± 120	140 ± 50	200 ± 80	17 ± 6	700 ± 110	90 ± 15
TM18	2	10.4	296	4.6	670 ± NM	310 ± 18	200 ± 130	440 ± NM	140 ± NM	15 ± 3	400 ± 160	91 ± NM
TM19	1	3.0	232	4.2	580 ± NM	260 ± NM	200 ± NM	240 ± NM	150 ± NM	7 ± NM	130 ± NM	79 ± NM
TM20	1	33.4	138	5.3	600 ± NM	290 ± NM	290 ± NM	cont ± NM	99 ± NM	cont ± NM	380 ± NM	130 ± NM
MA8	2	3.8	359	2.4	NM ± NM	3820 ± 28	11000 ± 900	500 ± 160	120 ± 50	1100 ± 800	390 ± 13	NM ± NM
MA9	2	3.2	338	2.3	2300 ± NM	4900 ± 500	14000 ± 3000	200 ± 26	400 ± 15	300 ± 16	400 ± 80	120 ± NM
MA10	1	48.1	109	5.2	NM ± NM	22 ± NM	cont. ± NM	cont ± NM	cont ± NM	cont ± NM	cont ± NM	NM ± NM
MA11	1	3.7	328	2.2	3100 ± NM	4400 ± NM	11900 ± NM	290 ± NM	210 ± NM	340 ± NM	650 ± NM	220 ± NM
MA12	2	2.9	350	2.3	2900 ± NM	4500 ± NM	12300 ± NM	310 ± NM	620 ± NM	300 ± NM	650 ± NM	170 ± NM
MA13	2	18.1	140	2.6	600 ± 260	6090 ± 50	2340 ± 50	200 ± 20	900 ± 500	17 ± 11	1500 ± NM	90 ± 13
MA14	2	2.6	319	2.3	900 ± 230	5600 ± 80	6730 ± 70	220 ± 12	500 ± 270	109 ± 1	1800 ± 100	280 ± 20
MA15	2	1.4	354	2.7	1600 ± 300	4400 ± 110	12500 ± 500	260 ± 60	320 ± 21	240 ± 13	390 ± 27	180 ± 15
MA16	2	2.1	364	2.7	2600 ± 400	4610 ± 18	14000 ± 300	250 ± 17	1100 ± 600	210 ± 7	500 ± 120	140 ± 11
MA17	2	8.0	362	2.8	1300 ± 600	3700 ± 120	13000 ± 2500	500 ± 130	560 ± 21	500 ± NM	700 ± 110	200 ± 9
MA18	2	12.8	300	2.7	1200 ± NM	4500 ± 110	11190 ± 27	260 ± NM	640 ± NM	160 ± 70	300 ± 300	130 ± 70
MA19	2	9.4	308	2.9	1600 ± 160	4500 ± 90	10980 ± 40	320 ± 50	840 ± NM	600 ± 160	534 ± 4	200 ± 22
MA20	2	2.7	344	2.6	1200 ± 20	5080 ± 60	11800 ± 300	200 ± 10	440 ± 50	170 ± 40	400 ± 110	150 ± 16
MA21	2	2.8	345	2.7	1100 ± 300	4360 ± 3	12200 ± 40	250 ± 11	340 ± 11	260 ± 50	400 ± 80	150 ± 40

Endmember compositions of hydrothermal vent fluids based on extrapolation to Mg = 0 (Von Damm et al., 1985; Trefry et al., 1994; Metz and Trefry, 2000). Uncertainties reflect the

TMo = Taho Moana-1; A = ABE; TM = Tu'i Malila; MA = Mariner

n = number of vent fluid sample replicates; mm = mmol/kg; µm = µmol/kg; nm = nmol/kg

NM = not measured; cont = contaminated

Table 8 (continued).

Endmember Metal Concentrations of Hydrothermal Vent Fluids from the Eastern Lau Spreading Center and Valu Fa Ridge.

Fluid	n =	min. Mg	max. T	min. pH	Mo	Ag	Cd	In	Sn	Sb	Au	Pb
		mm	°C	(25°C)	nm	nm	nm	nm	nm	nm	nm	nm
TMo1	2	2.4	306	3.3	100 ± 40	40 ± 12	210 ± 20	NM ± NM	6 ± NM	40 ± 15	0 ± NM	530 ± NM
TMo2	2	1.0	298	3.9	90 ± 19	45 ± 4	120 ± 60	NM ± NM	6 ± NM	40 ± 10	0 ± NM	300 ± 200
TMo5	2	1.4	310	3.7	43 ± 6	26 ± 1	96 ± 1	NM ± NM	1 ± NM	28 ± 6	0 ± NM	58 ± 0.9
A10	1	2.1	317	4.4	41 ± NM	14 ± NM	31 ± NM	NM ± NM	3 ± NM	51 ± NM	0 ± NM	370 ± NM
A11	2	2.1	312	3.9	68 ± 4	6 ± 3	39 ± 7	NM ± NM	2 ± 0	19 ± 5	0 ± 0.03	200 ± 100
A13	2	2.3	283	4.3	1500 ± 170	50 ± 21	160 ± NM	50 ± 12	50 ± 40	59 ± NM	1600 ± 400	480 ± NM
A14	2	1.9	300	4.0	1400 ± NM	40 ± 40	600 ± NM	57 ± 3	90 ± 13	170 ± NM	820 ± NM	550 ± NM
A15	2	1.9	290	4.4	400 ± 400	51 ± NM	110 ± 21	30 ± 15	50 ± 13	100 ± NM	240 ± NM	900 ± 270
A16	2	1.7	263	4.5	900 ± 90	bdl ± NM	54 ± 4	40 ± 4	90 ± 50	44 ± 6	700 ± 400	600 ± 140
TM11	2	1.1	315	3.8	200 ± 110	20 ± 8	76 ± 7	NM ± NM	50 ± 40	36 ± 7	0 ± NM	900 ± 400
TM12	2	3.0	284	4.2	115 ± 4	33 ± 2	300 ± 220	NM ± NM	NM ± NM	40 ± 13	1 ± NM	2000 ± 900
TM13	2	3.6	262	3.9	1100 ± 200	14 ± 3	160 ± 24	45 ± NM	40 ± 4	49 ± 1	2100 ± 210	400 ± 300
TM14	2	1.5	290	3.9	1200 ± 250	16 ± 4	160 ± 11	50 ± 15	68 ± 3	60 ± 16	3000 ± 2985	1000 ± 210
TM15	1	22.0	269	5.0	cont ± NM	cont ± NM	cont ± NM	cont ± NM	cont ± NM	cont ± NM	cont ± NM	cont ± NM
TM16	2	5.5	251	3.9	2200 ± 140	120 ± NM	1600 ± 700	46 ± 2	60 ± 16	110 ± 50	2500 ± 600	2000 ± 1400
TM17	2	3.1	258	3.9	1260 ± 50	100 ± 30	1200 ± 120	44 ± 4	41 ± 5	120 ± 50	2700 ± 300	3300 ± 140
TM18	2	10.4	296	4.6	1400 ± NM	2 ± 1	1400 ± 600	56 ± NM	56 ± NM	80 ± 50	5000 ± 1000	1300 ± 230
TM19	1	3.0	232	4.2	1200 ± NM	520 ± NM	130 ± NM	50 ± NM	48 ± NM	460 ± NM	8700 ± NM	11500 ± NM
TM20	1	33.4	138	5.3	cont ± NM	20 ± NM	800 ± NM	cont ± NM	cont ± NM	130 ± NM	7600 ± NM	2200 ± NM
MA8	2	3.8	359	2.4	300 ± 80	50 ± 18	287 ± 0	NM ± NM	NM ± NM	1790 ± 14	1 ± NM	1100 ± 300
MA9	2	3.2	338	2.3	230 ± NM	66 ± NM	450 ± NM	NM ± NM	NM ± NM	1900 ± 900	1 ± NM	1200 ± NM
MA10	1	48.1	109	5.2	cont ± NM	cont ± NM	cont ± NM	NM ± NM	NM ± NM	280 ± NM	cont ± NM	cont ± NM
MA11	1	3.7	328	2.2	220 ± NM	59 ± NM	310 ± NM	NM ± NM	NM ± NM	1800 ± NM	1 ± NM	2500 ± NM
MA12	2	2.9	350	2.3	160 ± NM	96 ± NM	490 ± NM	NM ± NM	NM ± NM	98 ± NM	2 ± NM	5400 ± NM
MA13	2	18.1	140	2.6	1500 ± 300	51 ± NM	180 ± NM	61 ± 7	63 ± NM	100 ± 40	1800 ± 500	cont ± NM
MA14	2	2.6	319	2.3	700 ± 400	40 ± 28	1560 ± 40	160 ± 18	88 ± 28	140 ± 16	3000 ± 900	2000 ± 1000
MA15	2	1.4	354	2.7	1470 ± 70	60 ± 15	350 ± 15	90 ± 8	78 ± 2	110 ± 22	2000 ± 900	1400 ± 150
MA16	2	2.1	364	2.7	900 ± 270	50 ± 29	400 ± 150	84 ± 3	100 ± 40	170 ± NM	2400 ± 200	2200 ± 600
MA17	2	8.0	362	2.8	1300 ± 400	100 ± 14	400 ± 100	150 ± 28	90 ± 40	130 ± 70	28000 ± 2000	540 ± NM
MA18	2	12.8	300	2.7	1200 ± NM	100 ± NM	230 ± NM	110 ± 50	60 ± NM	140 ± NM	1500 ± NM	700 ± 300
MA19	2	9.4	308	2.9	1400 ± NM	90 ± 11	480 ± 28	240 ± 50	110 ± 3	360 ± 10	2200 ± NM	1200 ± NM
MA20	2	2.7	344	2.6	1200 ± 15	80 ± 40	400 ± 80	90 ± 14	55 ± 4	130 ± 30	2100 ± 600	1500 ± 500
MA21	2	2.8	345	2.7	1300 ± 260	50 ± 15	400 ± 90	100 ± 25	93 ± 23	160 ± 40	1100 ± 600	900 ± 150